Please cite this article in press as: Zhou et al., UHRF1 interacts with snRNAs and regulates alternative splicing in mouse spermatogonial stem cells, Stem Cell Reports (2022), https://doi.org/10.1016/j.stemcr.2022.06.010

Stem Cell Reports
Article
ISSCR
OPEN ACCESS

UHRF1 interacts with snRNAs and regulates alternative splicing in mouse spermatogonial stem cells

Shumin Zhou,[1,6] Juan Dong,[1,2,6] Mengneng Xiong,[1] Shiming Gan,[1] Yujiao Wen,[1] Jin Zhang,[1] Xiaoli Wang,[1] Shuiqiao Yuan,[1,3,4,*] and Yaoting Gui[5,*]

[1]Institute of Reproductive Health, Tongji Medical College, Huazhong University of Science and Technology, Wuhan, Hubei, China
[2]Department of Obstetrics and Gynecology, Union Hospital, Tongji Medical College, Huazhong University of Science and Technology, Wuhan, Hubei, China
[3]Laboratory Animal Center, Huazhong University of Science and Technology, Wuhan, Hubei 430030, China
[4]Shenzhen Huazhong University of Science and Technology Research Institute, Shenzhen, Guangdong 518057, China
[5]Guangdong Key Laboratory of Male Reproductive Medicine and Genetics, Institute of Urology, Peking University Shenzhen Hospital, Shenzhen PKU-HKUST Medical Center, Shenzhen, Guangdong 518036, China
[6]These authors contributed equally
*Correspondence: shuiqiaoyuan@hust.edu.cn (S.Y.), guiyaoting2007@aliyun.com (Y.G.)
https://doi.org/10.1016/j.stemcr.2022.06.010

SUMMARY

Life-long male fertility relies on exquisite homeostasis and the development of spermatogonial stem cells (SSCs); however, the underlying molecular genetic and epigenetic regulation in this equilibrium process remains unclear. Here, we document that UHRF1 interacts with snRNAs to regulate pre-mRNA alternative splicing in SSCs and is required for the homeostasis of SSCs in mice. Genetic deficiency of UHRF1 in mouse prospermatogonia results in gradual loss of spermatogonial stem cells, eventually leading to Sertoli-cell-only syndrome (SCOS) and male infertility. Comparative RNA-seq data provide evidence that *Uhrf1* ablation dysregulates previously reported SSC maintenance- and differentiation-related genes. We further found that UHRF1 could act as an alternative RNA splicing regulator and interact with *Tle3* transcripts to regulate its splicing event in spermatogonia. Collectively, our data reveal a multifunctional role for UHRF1 in regulating gene expression programs and alternative splicing during SSC homeostasis, which may provide clues for treating human male infertility.

INTRODUCTION

Spermatogonial stem cells (SSCs) are male germ cells located in the basal membrane of seminiferous tubules in testes (de Rooij, 2017). As the only stem cells in the male germ line, SSCs can self-renew to sustain a relatively steady number or differentiate and undergo mitosis, meiosis, and spermiogenesis to support continuous sperm production (de Rooij, 2017). Spermatogonial homeostasis includes self-renewal and differentiation, which are delicately regulated by epigenetic factors, including DNA methylation and histone modification (Zhou et al., 2021). Previous studies have identified several critical RNA-binding proteins, such as DND165, DDX5, and BCAS220, in SSCs, and each has a unique and dominant role in post-transcriptional regulation, hinting that this process is particularly evident in the regulation of alternative splicing and sustaining the continuous production of sperm and male fertility (Legrand et al., 2019; Liu et al., 2017; Yamaji et al., 2017; Zhou et al., 2015).

Alternative splicing (AS) is a key step in the splicing of pre-mRNA that largely enriches proteomic diversity (Nilsen and Graveley, 2010; Wang et al., 2008). In organisms, a substantial fraction of genes is strictly regulated by AS. The same gene is often expressed as different splicing isoforms in various tissues and cells or at different developmental stages of the same tissue. Abnormal splicing regulation is closely related to multiple biological processes, such as cellular migration and cell-cycle progression (Baralle and Giudice, 2017; Dominguez et al., 2016; Oltean and Bates, 2014). The splicing of pre-mRNA is executed by the spliceosome, which requires the interplay of *trans*-acting factors, including uracil-rich small ribonucleic acid-proteins (U1, U2, U4/U6, and U5) and small nuclear ribonucleoproteins (snRNPs) (Ule and Blencowe, 2019). Precise control of pre-mRNA splicing is integral during spermatogenesis, and various RNA-binding proteins have long been known, particularly at meiotic and post-meiotic stages (Legrand and Hobbs, 2018). However, only the tip of the iceberg regarding the regulatory mechanisms and functions of RNA-binding factors as key determinants of SSC homeostasis has been explored.

UHRF1 (also known as NP95 or ICBP90) is best known for its function in epigenetic regulation in multiple biological processes, including male germ cell meiosis and early embryo development (Cao et al., 2019; Chen et al., 2013; Dong et al., 2019; Muto et al., 2002, 2006; Newkirk and An, 2020; Pan et al., 2020; Takada et al., 2021; Tien et al., 2011; Wu et al., 2020). It has a powerful effect on the regulation of DNA-related epigenetic modifications, but its role in RNA metabolism is largely unexplored. Interestingly, a recent study reported that UHRF1 could interact with

Please cite this article in press as: Zhou et al., UHRF1 interacts with snRNAs and regulates alternative splicing in mouse spermatogonial stem cells, Stem Cell Reports (2022), https://doi.org/10.1016/j.stemcr.2022.06.010

splicing factors and may serve as a novel alternative RNA splicing regulator in cell lines *in vitro* (Xu et al., 2021). However, how UHRF1 regulates RNA splicing in mammalian cells *in vivo*, especially in male germ cells, remains elusive.

In this study, we, for the first time, identify that UHRF1 interacts with snRNAs to regulate pre-mRNA AS in SSCs and is essential for the homeostasis and maintenance of SSCs in mice. We found that UHRF1 is highly expressed in SSCs and governs the transition from SSCs to a differentiated state in the male germ line. Conditional inactivation of UHRF1 in prospermatogonia (*Vasa-Cre* induced) significantly affects SSC differentiation after birth and ultimately leads to a Sertoli-cell-only syndrome in adult mice. Strikingly, we found, by immunoprecipitation and mass spectrometry (IP/MS) assay in SSCs, that a large proportion of UHRF1-interacting proteins are related to RNA splicing processes. Through RNA immunoprecipitation (RIP)-PCR approaches, we confirmed that UHRF1 has a high binding intensity on snRNAs and pre-mRNAs that regulate SSC homeostasis. Furthermore, deletion of UHRF1 results in a significant misregulation of AS events in SSCs, especially skipped exons. These data uncover a novel molecular function of UHRF1 that binds to RNA and regulates AS in SSCs, which adds another layer to the role of UHRF1 in stem cell and male germline development.

RESULTS

Expression profiles of UHRF1 in mouse spermatogonia

To explore the function of UHRF1 in SSCs, we first examined the localization of UHRF1 in spermatogonia using co-immunostaining of UHRF1 with PLZF (a marker of undifferentiated spermatogonia). The results showed that UHRF1 was expressed in the nucleus of PLZF-positive undifferentiated spermatogonia in both postnatal day 1 (P1) and adult mouse testes (Figures 1A and 1B). Interestingly, it manifested heterogeneous expression in undifferentiated spermatogonia (Figure S1A), displaying bright signals, dim signals, and no signals. According to the fragmentation model, undifferentiated spermatogonia can be subdivided into GFRα1-positive SSCs and RARγ1-positive spermatogonial progenitor cells (SPCs) (La et al., 2018; Nakagawa et al., 2010). To define the classification and identification of UHRF1-positive undifferentiated spermatogonia, we stained the cross sections with antibodies against GFRα1 and RARγ1. Surprisingly, UHRF1 was present in both GFRα1$^+$ SSCs and RARγ1$^+$ SPCs (Figures 1C and S1B). Then, we utilized a published undifferentiated spermatogonia scRNA-seq dataset (Hermann et al., 2018) to investigate the expression pattern of UHRF1 at the RNA level. We identified 14 cell clusters, with clusters 2, 3, 10, and 12 designated SSCs and clusters 0, 1, and 8 defined as SPCs (Figures S1C and S1D). Consistent with the expression pattern of UHRF1 at the protein level revealed by immunofluorescence, *Uhrf1* was expressed in all clusters, including SSCs and SPCs, and was expressed heterogeneously in each cluster (Figures 1D and S1C–S1E). Together, these results indicate that UHRF1 was enriched in undifferentiated spermatogonia and showed heterogeneous expression in different spermatogonial cell types.

Ablation of UHRF1 in prospermatogonia results in male infertility

To systematically elucidate the role of UHRF1 during spermatogenesis, particularly in spermatogonia, we generated a conditional knockout mouse model in which *Uhrf1* exon 4 was flanked with *LoxP* sites and *Uhrf1* was excised specifically in germ cells at embryonic day (E15.5) by *Vasa*-Cre (Figure 2A). We found that UHRF1 was lost in the germ cells of *Uhrf1*$^{flox/-}$;*Vasa*-Cre mice at P1 and P5 (Figures 2B–2D and S2A). *Uhrf1*$^{flox/-}$;*Vasa*-Cre males were sterile and produced no pups when co-caged with either *Uhrf1*$^{flox/flox}$ or *Uhrf1*$^{+/flox}$;*Vasa*-Cre females. Similarly, *Uhrf1*$^{flox/-}$;*Vasa*-Cre female mice were also infertile when bred with either genotype of male mice, indicating that UHRF1 is essential for fertility in male and female mice (Figure 2E). Consistent with this infertile phenotype, the testis-to-body weight ratios of *Uhrf1*$^{flox/-}$;*Vasa*-Cre male mice significantly decreased from P5 compared with controls (Figure 2F). We then examined the histology of *Uhrf1*$^{flox/-}$;*Vasa*-Cre testes at various postnatal time points (P5, P7, P9, P12, P15) and found that the diameter of seminiferous tubules was decreased from P5 (Figure S2B). Moreover, adult *Uhrf1*$^{flox/-}$;*Vasa*-Cre mouse seminiferous tubules were agametic and resembled a Sertoli-cell-only syndrome in humans, and no round or elongating spermatids were observed in the cauda or corpus epididymis of *Uhrf1*$^{flox/-}$;*Vasa*-Cre male mice (Figure 2G). These data indicate that UHRF1 ablation in prospermatogonia causes germ cell loss and male sterility and might function in spermatogonial development.

UHRF1 is essential for spermatogonial differentiation and SSC maintenance

To assess the function of UHRF1 in spermatogonial development, we calculated the STRA8 (a marker for differentiating spermatogonia)- and γ-H2AX-positive germ cells in both control and *Uhrf1*$^{flox/-}$;*Vasa*-Cre mouse testes at different ages. We found that the number of STRA8-positive spermatogonia was decreased as early as P5, when just a small number of STRA8-positive spermatogonia emerged in the control cross section of seminiferous tubules (Figures 3A and 3B). A significantly reduced number of γ-H2AX-positive germ cells was observed at either P12 or P15 in *Uhrf1*$^{flox/-}$;*Vasa*-Cre mouse testes (Figures 3A

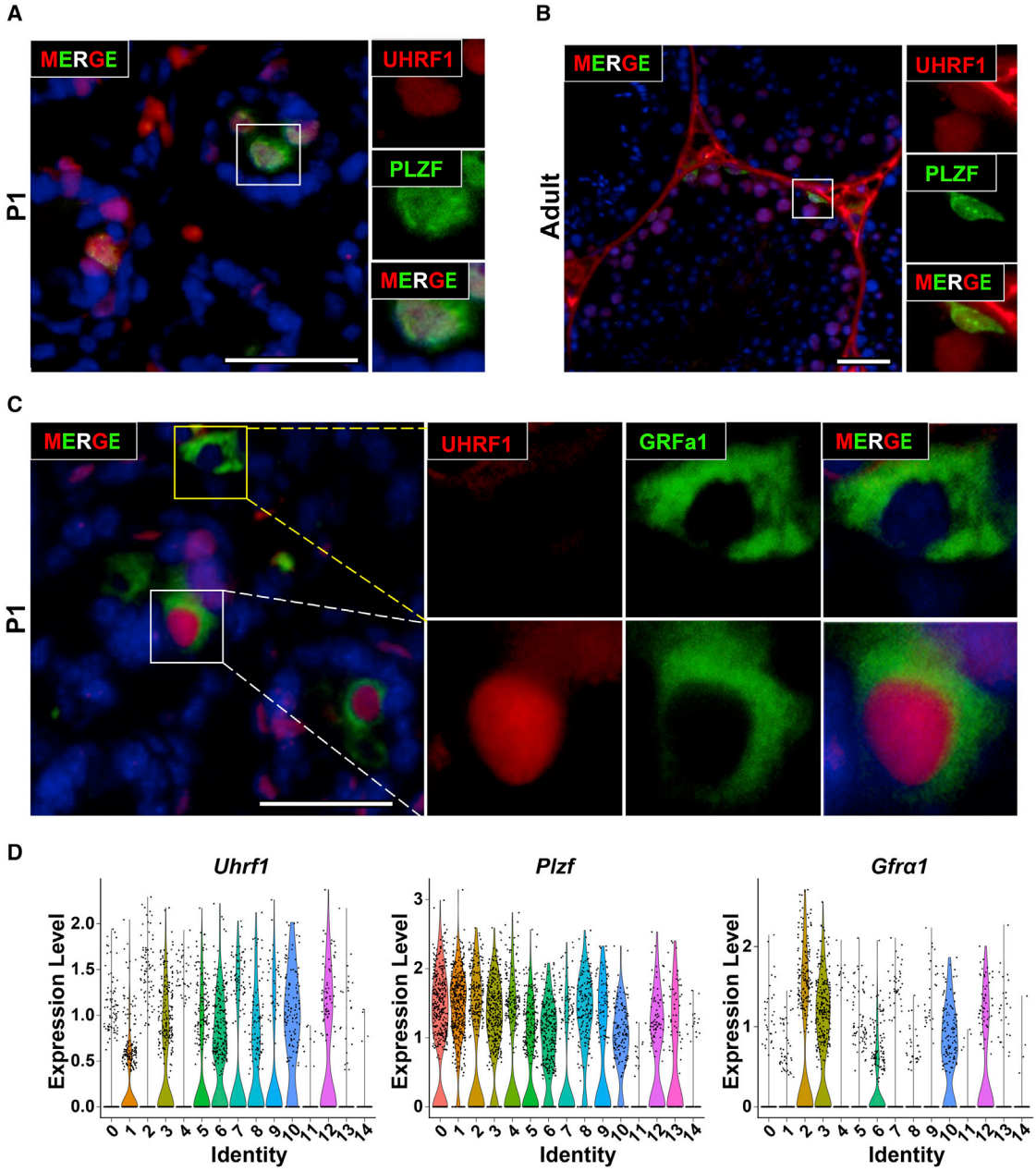

Figure 1. Dynamic expression of UHRF1 in mouse spermatogonia

(A and B) Representative co-immunofluorescence images of PLZF (green) and UHRF1(red) on postnatal day 1 (P1) (A) and adult testis (B) sections. Scale bars, 50 μm.

(C) Representative immunofluorescence images of seminiferous tubules at P1 stained for GFRα1 (green) and UHRF1(red). Scale bar, 50 μm.

(D) Violin plots of published scRNA-seq data showing the gene expression patterns of *Uhrf1* and selected spermatogonia marker genes (*Plzf* and *Gfrα1*).

and 3C). Moreover, ~59.1% of *Uhrf1*$^{flox/-}$;*Vasa*-Cre mouse seminiferous tubules at P15 manifested "empty tubules" (STRA8-negative or γ-H2AX-negative tubules), indicating that the spermatogonia failed to enter differentiation and meiosis (Figures 3D and 3E).

Since we observed a Sertoli-cell-only syndrome in adult *Uhrf1*$^{flox/-}$;*Vasa*-Cre mouse testes (Figure 2G), we next asked whether the developmental efficiency of spermatogonia was affected. Immunofluorescence confirmed that the number of PLZF-positive cells (undifferentiated spermatogonia) was

Please cite this article in press as: Zhou et al., UHRF1 interacts with snRNAs and regulates alternative splicing in mouse spermatogonial stem cells, Stem Cell Reports (2022), https://doi.org/10.1016/j.stemcr.2022.06.010

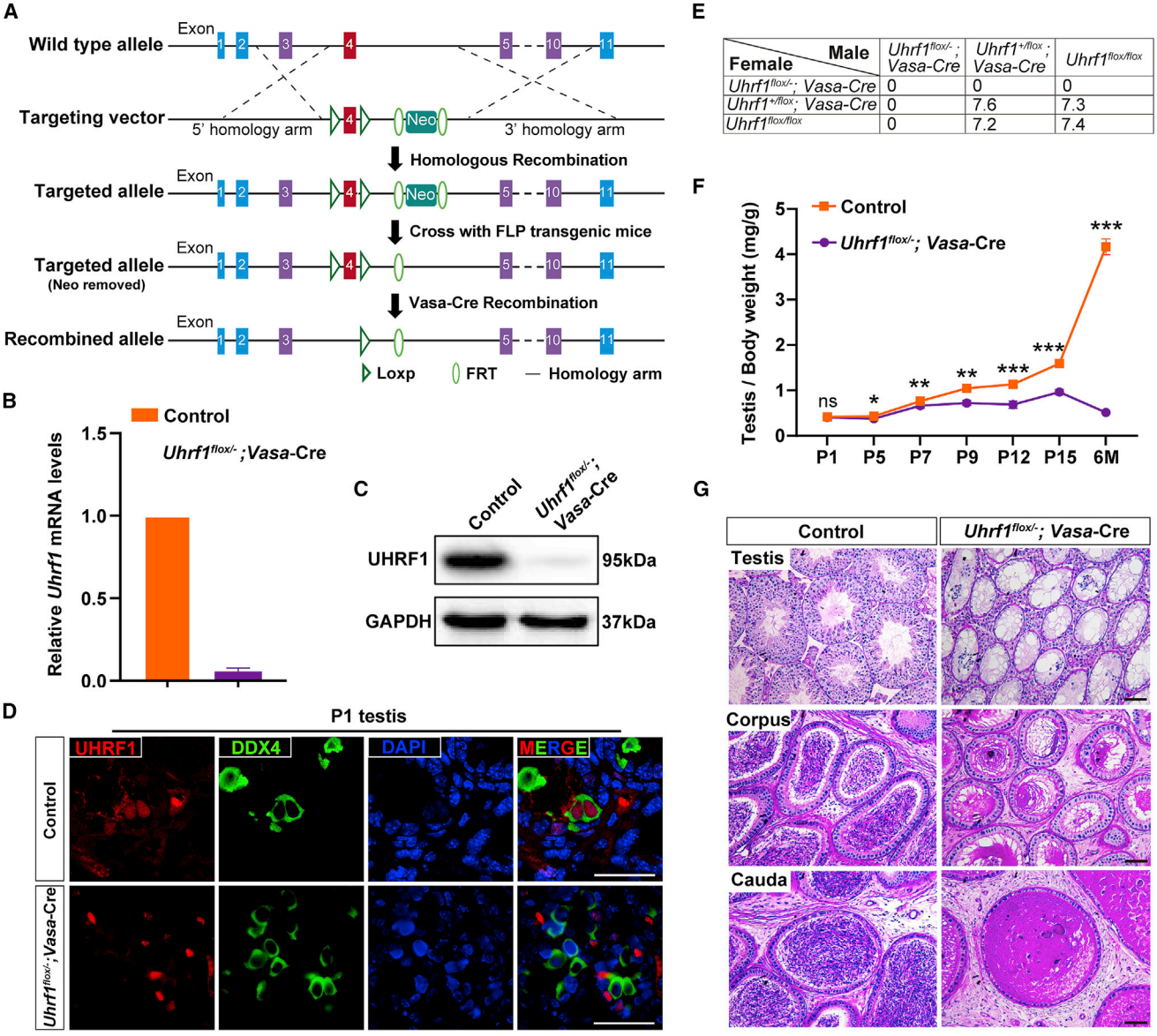

Figure 2. *Uhrf1* deletion in prospermatogonia results in germ cell degeneration

(A) Schematic diagram of the targeting strategy for generating a floxed *Uhrf1* allele through homologous recombination in murine embryonic stem cells. Exon 4 will be deleted after Cre-mediated recombination.

(B–D) Representative RT-qPCR, western blots, and immunofluorescence depicting the mRNA and protein levels of *Uhrf1* in $Uhrf1^{flox/-}$;*Vasa*-Cre mouse testes compared with those of controls. Blots are representative of n = 3 independent experiments. Scale bars, 50 μm.

(E) $Uhrf1^{flox/-}$;*Vasa*-Cre, $Uhrf1^{+/flox}$;*Vasa*-Cre, and $Uhrf1^{flox/flox}$ male and female mice were mated with more than three pairs to perform fertility tests. Mean litter sizes are shown with the indicated genotypes.

(F) Testis growth curve indicates that the $Uhrf1^{flox/-}$;*Vasa*-Cre testes were significantly decreased from P5. Data are presented as the mean ± SEM; n = 3; *p < 0.05, **p < 0.01, ***p < 0.001.

(G) Periodic acid-Schiff (PAS) staining of adult testis and epididymis (cauda and corpus) sections from $Uhrf1^{flox/-}$;*Vasa*-Cre and control mice. Scale bars, 50 μm.

substantially reduced in $Uhrf1^{flox/-}$;*Vasa*-Cre mouse seminiferous tubules by P5, P7, P12, and P15 (Figures 4A and 4B). As the undifferentiated spermatogonia (PLZF-positive cells) include SSCs and SPCs, we examined the identity of progenitors by immunofluorescence for RARγ1 (progenitor-associated marker). The results showed that RARγ1-positive spermatogonia decreased significantly at P7 and were largely absent at P12 in $Uhrf1^{flox/-}$;*Vasa*-Cre seminiferous tubules

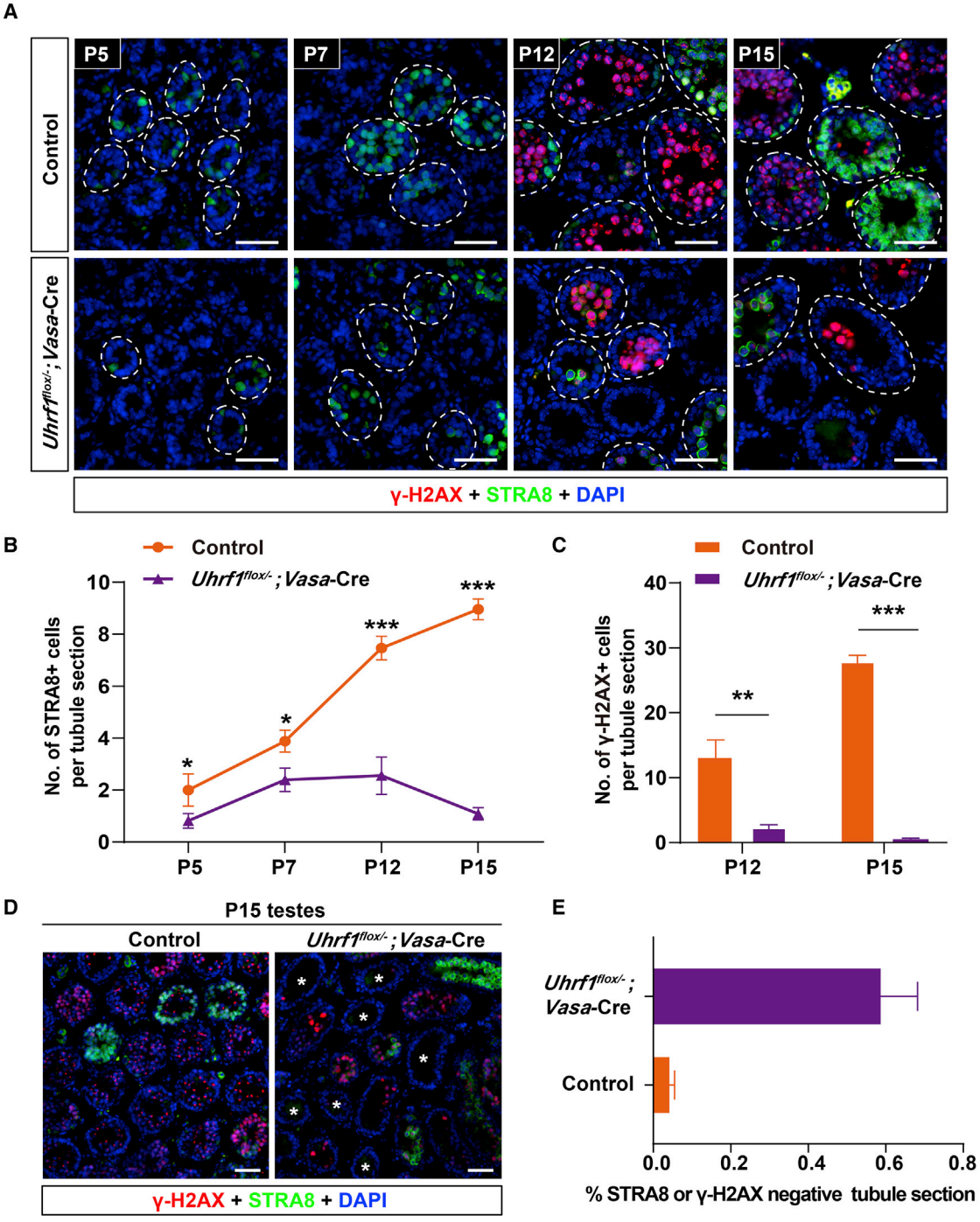

Figure 3. Critical role of UHRF1 in spermatogonial differentiation

(A) Co-immunofluorescence staining for γ-H2AX (red) and STRA8 (green) on control and *Uhrf1*$^{flox/-}$;*Vasa*-Cre testis sections at P5, P7, P12, and P15. Scale bar, 50 μm. White dashed lines indicate the single seminiferous tubule.

(B and C) Quantification of STRA8-positive cells (B) and γ-H2AX-positive cells (C) per cross section in (A). Data are presented as the mean ± SEM; n = 3; *p < 0.05, **p < 0.01, ***p < 0.001.

(D) The co-immunofluorescence staining of γ-H2AX (red) and STRA8 (green) on control and *Uhrf1*$^{flox/-}$;*Vasa*-Cre testis sections at P15. The asterisks (*) mark tubules that lack γ-H2AX and STRA8 signals. Scale bar, 50 μm.

(E) Quantification of the percentage of STRA8- or γ-H2AX-negative tubules for (D) is shown. Data are presented as the mean ± SEM; n = 3.

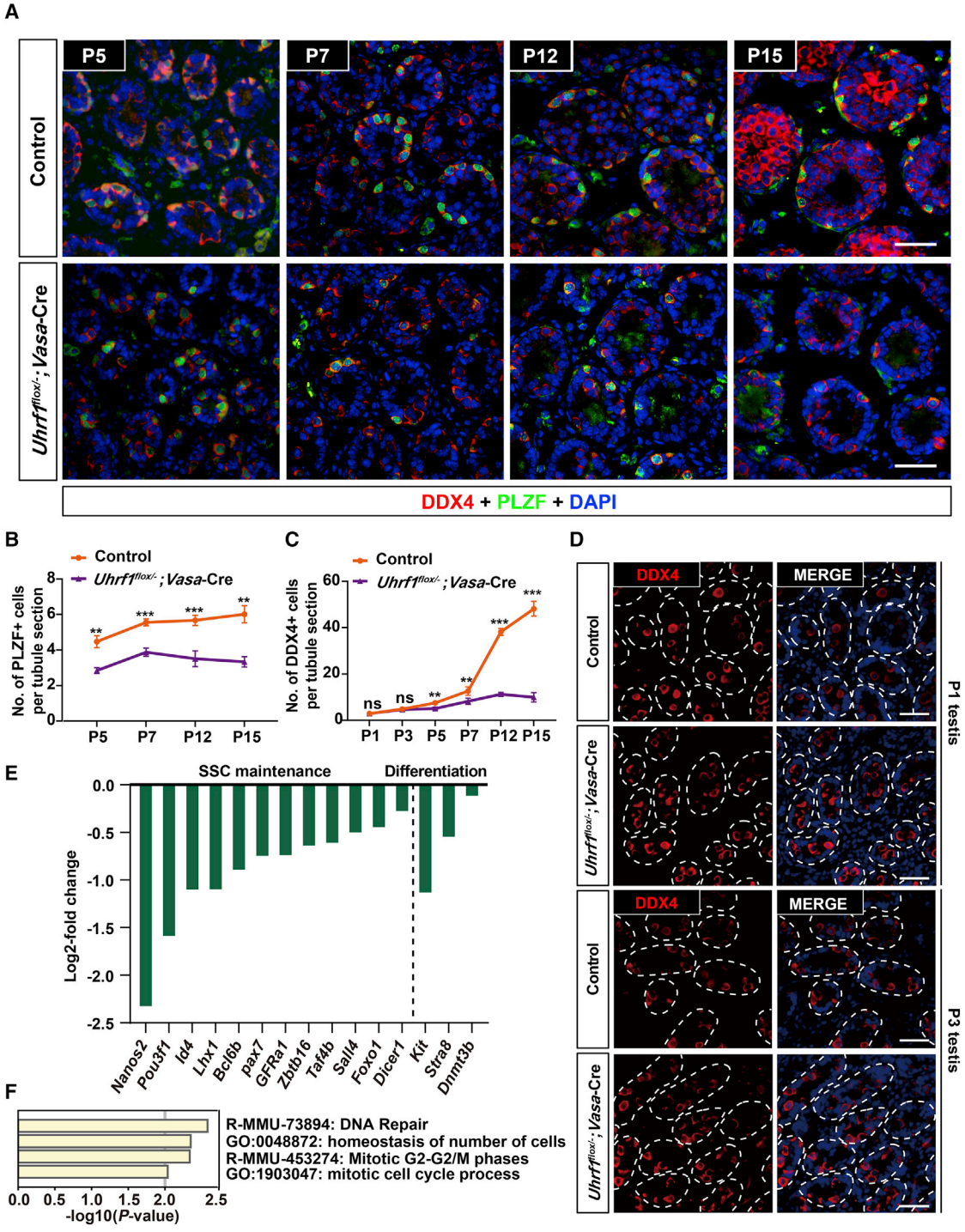

Figure 4. UHRF1 is essential for maintenance of undifferentiated spermatogonia

(A) Co-immunofluorescence staining for DDX4 (red) and PLZF (green) on control and *Uhrf1*$^{flox/-}$;*Vasa*-Cre testis sections at P5, P7, P12, and P15. Scale bars, 50 μm.

(B and C) Quantification of PLZF-positive cells (B) and DDX4-positive cells (C) per tubule for (A). Data are presented as the mean ± SEM; n = 3; **p < 0.01, ***p < 0.001.

(legend continued on next page)

compared with the controls (Figures S2C and S2D), indicating that progenitor populations were affected upon UHRF1 deletion in prospermatogonia. Given that prospermatogonia re-entered mitosis and generated spermatogonia shortly after birth, we determined the overall number of germ cells at P1 and P3 testes in control and *Uhrf1*$^{flox/-}$;*Vasa*-Cre mice by staining with an antibody against DDX4. Interestingly, the number of DDX4-positive germ cells was comparable between control and *Uhrf1*$^{flox/-}$;*Vasa*-Cre testes at both P1 and P3 (Figures 4C and 4D). These results suggest that the loss of undifferentiated spermatogonia in *Uhrf1*$^{flox/-}$;*Vasa*-Cre mice might be caused by the disruption of SSC maintenance rather than the failure of prospermatogonia-to-spermatogonia transition.

To explore the cause of spermatogonia loss, we performed terminal deoxynucleotidyl transferase-mediated deoxyuridine triphosphate (TUNEL) assays in control and *Uhrf1*$^{flox/-}$;*Vasa*-Cre mouse testes at P5 and P7, when spermatogonia are enriched and no spermatocytes are produced. Unexpectedly, no significant apoptosis was observed in P5 and P7 mutant testes, which indicates that the loss of spermatogonia was not due to increased apoptosis (Figures S3A and S3B). Then, we chose the time points of P12 and P15 in testes, when spermatocytes emerged. We found that *Uhrf1*$^{flox/-}$;*Vasa*-Cre mouse testes at P12 contained elevated apoptotic cells, and more severe apoptosis was observed at P15 (Figures S3A and S3B). Moreover, the percentages of Ki67$^+$ SALL4$^+$ spermatogonia of the remaining SALL4$^+$ spermatogonia were comparable between control and mutant testes at P7 (Figures S3C and S3D), suggesting that the block of spermatogonial differentiation is not due to a lower proliferation of SSCs. Taken together, the above observations reveal that UHRF1 ablation in prospermatogonia results in aberrant spermatogonial differentiation and SSC maintenance, thereby leading to a dramatic loss of spermatogonia and spermatogenic cells that disturbs the first wave of spermatogenesis after birth.

RNA-seq reveals an abnormal transcriptome as a result of UHRF1 loss in prospermatogonia

To determine the molecular consequences of the loss of UHRF1 in prospermatogonia, we compared the transcriptomes of control and *Uhrf1*$^{flox/-}$;*Vasa*-Cre testes at P0 and P7. RNA-sequencing (RNA-seq) analyses identified 13 upregulated and 22 downregulated genes at P0 using $|\log_2(\text{fold change})| > 1$ and $p < 0.05$ (Figure S4A; Tables S1 and S2). Using the same criterion, we identified 81 genes that were upregulated and 70 that were downregulated in *Uhrf1*$^{flox/-}$;*Vasa*-Cre testes at P7 compared with controls (Figure S4B). Strikingly, RNA-seq and qRT-PCR analyses confirmed that selected genes associated with SSC maintenance and differentiation tended to be downregulated, although some changes were not significant (Figures 4E and S4C). In addition, we performed gene ontology (GO) term enrichment analysis using all deregulated genes and found that these downregulated genes were associated with DNA repair, mitotic cell-cycle process, mitotic G2-G2/M phases, and homeostasis of the number of cells, which is consistent with the phenotype we observed in *Uhrf1*$^{flox/-}$;*Vasa*-Cre mice (Figure 4F). However, these upregulated genes were enriched for non-reproductive functions, such as herpes simplex infection, inner-ear development, and negative regulation of immune system processes (Figure S4D), which suggests that UHRF1 plays a role in silencing non-lineage-specific genes in testes. Therefore, these bioinformatics analyses imply that UHRF1 in spermatogonia may participate in the gene network regulation during the first wave of spermatogenesis.

UHRF1 interacts with snRNAs and snRNPs

To further explore the molecular function of UHRF1 in SSCs, we characterized UHRF1-interacting proteins by IP/MS analyses with isolated SSCs (Figure 5A). We identified 337 candidate proteins that interacted with UHRF1 and subjected these proteins to GO term, Kyoto Encyclopedia of Genes and Genomes (KEGG), and Protein-Protein Interaction Networks (PPI) analyses (Figure S5; Tables S3 and S4). Strikingly, the results showed that a large proportion of UHRF1-interacting proteins are the components of the spliceosome and participate in RNA splicing (Figure 5B). To gain additional insight into UHRF1 function in regulating AS, we chose 116 RNA-splicing-related proteins to perform GO term analyses. Interestingly, we observed that the most enriched GO terms were related to snRNPs (Figure 5C). Thus, we speculated that UHRF1 might exert a role in the regulation of RNA splicing events in SSCs. To substantiate this hypothesis, we performed an anti-UHRF1 RIP assay using P7 testes. As a substantial fraction of UHRF1-interacting proteins are snRNPs, we first examined whether UHRF1 could bind to U1, U2, U4, U5, and U6 snRNAs. Interestingly, we found that UHRF1 has a high binding intensity on U1, U2, and U4 snRNPs but no significant enrichment with the other two spliceosomal snRNAs (U5 and U6) (Figures 5D and 5E).

(D) Co-immunofluorescence staining for DDX4 on control and *Uhrf1*$^{flox/-}$;*Vasa*-Cre testis sections at P1 and P3. Scale bars, 50 μm. White dashed lines indicate the single seminiferous tubule.
(E) Histogram showing the RNA-seq results of selected transcripts ($\log_2$-fold change) associated with SSC maintenance and differentiation.
(F) Gene ontology of downregulated genes in P7 *Uhrf1*$^{flox/-}$;*Vasa*-Cre testes.

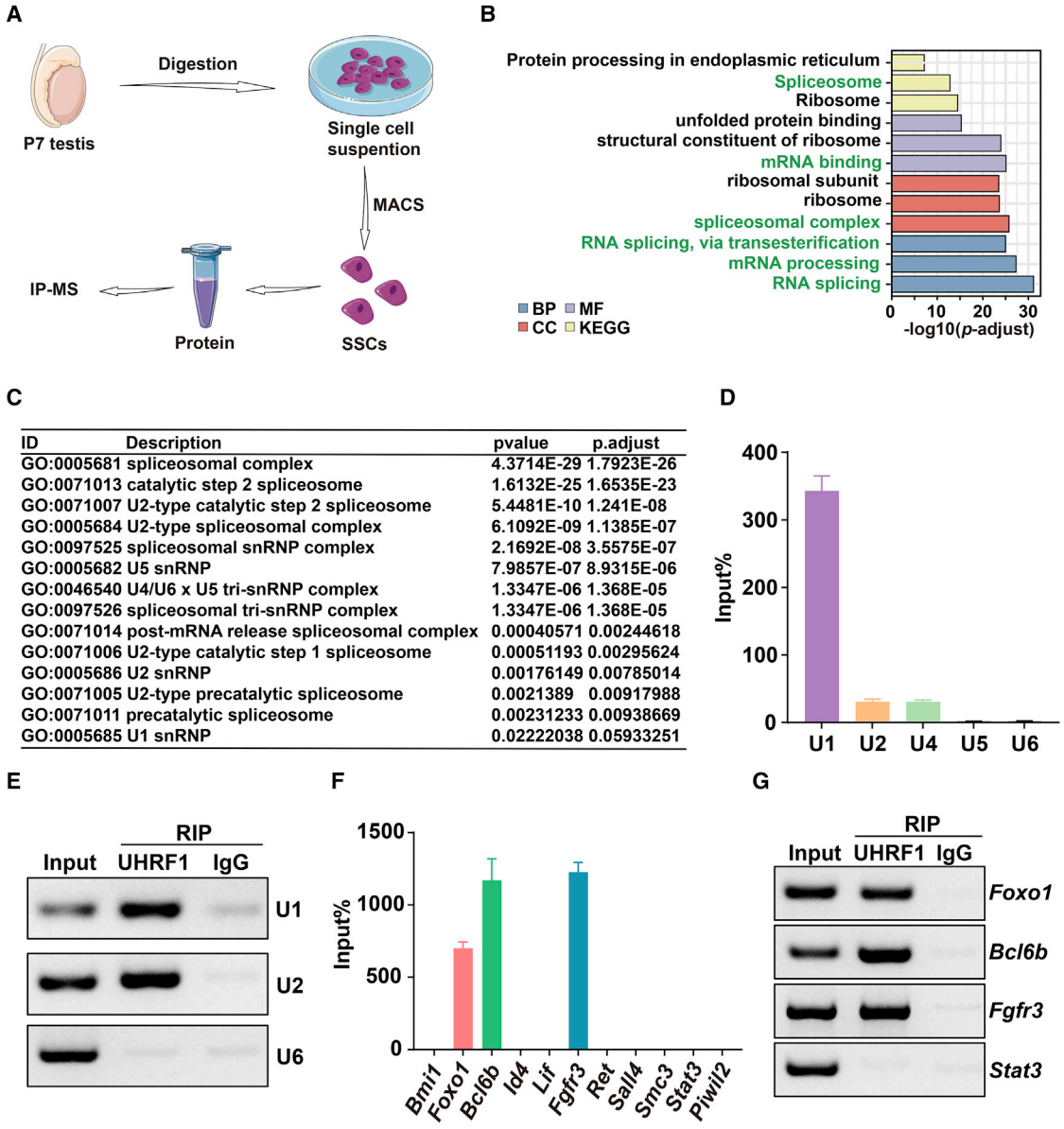

Figure 5. UHRF1 interacts with snRNA and spermatogonial maintenance-associated transcripts

(A) The schematic diagram shows the isolation of SSCs via MACS (magnetic-activated cell sorting) and the identification of interacting proteins.

(B) Gene ontology (GO) term enrichment and Kyoto Encyclopedia of Genes and Genomes (KEGG) analyses of UHRF1-bound proteins in isolated mouse SSCs are shown. BP, biological process; MF, molecular function; CC, cellular component.

(C) Gene ontology analysis of 116 RNA splicing-related proteins identified by UHRF1 IP-MS. The p value was obtained from the data by GOrilla analysis.

(D and E) Anti-UHRF1 RNA immunoprecipitation (RIP) coupled with qPCR (D) and PCR (E) assays showed significant U1, U2, and U4 snRNA enrichment but not that of U5 and U6 snRNAs.

(F and G) Anti-UHRF1 RIP coupled with qPCR (F) and PCR (G) showed UHRF1 binding to *Foxo1*, *Bcl6b*, and *Fgfr3* transcripts in mouse testis.

As above, UHRF1 was found to be essential for spermatogonial differentiation and SSC maintenance; we next asked whether UHRF1 has an enrichment on SSC homeostasis-related RNA. We chose several candidate genes that have been reported to play a role in the maintenance of SSC homeostasis (Wang et al., 2019) and found three gene transcripts (*Foxo1*, *Bcl6b*, and *Fgfr3*) that manifested a high binding intensity on anti-UHRF1 RNA precipitates

compared with the *Stat3* gene as a negative RIP control (Figures 5F and 5G). Of note, FOXO1, a marker of prospermatogonia and/or spermatogonia, localizes in the cytoplasm of prospermatogonia and gradually translocates from the cytoplasm to the nucleus in undifferentiated spermatogonia after birth. Combining this with the data that *Foxo1* was downregulated in knockout testes (Figures 4E and S4C), we asked whether UHRF1 exerts a regulatory role in FOXO1 expression in addition to the transcription and AS. We visualized the expression of FOXO1 by immunofluorescence and identified three types of FOXO1-positive cells in P7 mouse testes: cytoplasm only, nucleus only, and both cytoplasm and nucleus (Figure S6A). Surprisingly, we found that the efficiency of FOXO1 translocation from the cytoplasm to the nucleus was significantly reduced in *Uhrf1*$^{flox/-}$;*Vasa*-Cre mouse spermatogonia at both P7 and P12 compared with controls and that more mutant spermatogonia retained the cytoplasmic FOXO1 signal (Figures S6B–S6G). These findings suggested that UHRF1 regulates not only transcription and AS of the *Foxo1* gene but also the localization of FOXO1 protein. Taken together, our data indicate that UHRF1 could interact with snRNAs and snRNPs in testes as an RNA-binding protein, thereby regulating the expression of genes that are related to spermatogonial development.

UHRF1 regulates alternative splicing in testes

Given the findings that UHRF1 is involved with snRNAs and snRNPs, we sought to verify the role of UHRF1 in RNA splicing. By utilizing replicate multivariate analysis of transcript splicing (rMATS) analysis, we reanalyzed our RNA-seq data of P7 testes to identify AS events upon loss of UHRF1 in prospermatogonia. We discovered 1,141 AS events upon loss of UHRF1 in spermatogonia (false discovery rate [FDR] < 0.05, $|\Delta\psi| > 0.05$), with the majority of events (=758/1,141) annotated as a skipped exon (Figure 6A and Table S5). We then selected four candidate genes and validated these AS events by PCR analyses. The PCR results confirmed that loss of UHRF1 resulted in differential expression of exon 2 in *Apbb1* (increased exon skipping), exon 3 in *Senp7* (increased exon skipping), exons 7 and 8 in *Tle3* (increased exon skipping), and exon 3 in *Zfp808* (increased exon skipping) (Figures 6B and 6C). Moreover, RIP-PCR further showed that UHRF1 manifested a high enrichment on *Tle3* and a modest enrichment on *Zfp808*, revealing that UHRF1 is directly associated with the splicing of *Tle3* and *Zfp808* (Figure 6D). Other candidates such as *Apbb1* and *Senp7* were confirmed to be differentially spliced upon UHRF1 loss but showed slight or no binding to UHRF1, indicating that their splicing is indirectly regulated by UHRF1 (Figure 6D). Then we examined the mRNA expression levels of these four genes. Interestingly, the expression of these genes was dysregulated in *Uhrf1*$^{flox/-}$;*Vasa*-Cre mouse spermatogonia, indicating that UHRF1 has broad effects on these genes, including transcriptional regulation and post-transcriptional splicing (Figure S6H).

In addition, since *Tle3* has been reported to be associated with male reproduction (Lee et al., 2019), we next asked whether the exon 7/8 skipping alters the reading frame of *Tle3* mRNA and TLE3 protein expression in spermatogonia. We first utilized ORF FINDER to predict the open reading frame (ORF) of the *Tle3* exon-skipped isoform and found that the reading frame of *Tle3* mRNA was affected after undergoing AS (Figure S6I). Then we mapped the *Tle3* exon-skipped ORF to sequence databases using Smart BLAST and found that the *Tle3* exon-skipped variant was not included in the known protein sequence, indicating that exon-skipped *Tle3* mRNA may be decayed (Figure S6I). Further western blot analysis demonstrated that the protein expression level of TLE3 was decreased in *Uhrf1*$^{flox/-}$;*Vasa-Cre* mouse testes compared with controls, but the exon-skipped isoform was not detected (Figure S6J). Altogether, our data suggest that UHRF1 is involved in the regulation of RNA splicing events by interacting with snRNAs and snRNPs to directly and/or indirectly modulate gene expression in spermatogonia.

DISCUSSION

Mammalian spermatogenesis is a lifelong process that is maintained by equilibrium between self-renewing and differentiating SSCs. Disruption of this balance usually results in spermatogenic degeneration and male infertility. In this study, we identified UHRF1 as an important SSC homeostasis regulator that manifests dynamic expression in undifferentiated and differentiating spermatogonia. Exploiting a transgenic knockout model for UHRF1 in mice, we demonstrated that UHRF1 balances the self-renewal and differentiation of SSCs. UHRF1 deficiency disturbed the sustained cycles of spermatogenesis and led to Sertoli-cell-only syndrome (SCOS) in adult mice. Comparative RNA-seq data demonstrate that *Uhrf1* ablation dysregulates previously reported SSC maintenance- and differentiation-related genes. Our data provide evidence that UHRF1 is a critical factor in maintaining SSC homeostasis and demonstrate the role of UHRF1 in post-transcriptional gene regulation as a mediator of RNA splicing via interactions with pre-mRNAs, snRNAs, and other RNA-binding proteins, thereby maintaining the homeostasis of SSCs (Figure 6E).

UHRF1 was initially discovered in mouse and human cells as nuclear protein 95 (Fujimori et al., 1998; Hopfner et al., 2000) and quickly rose to a focal point as a multifunctional epigenetic regulator in diverse cellular and developmental processes. UHRF1 is best known for its function in

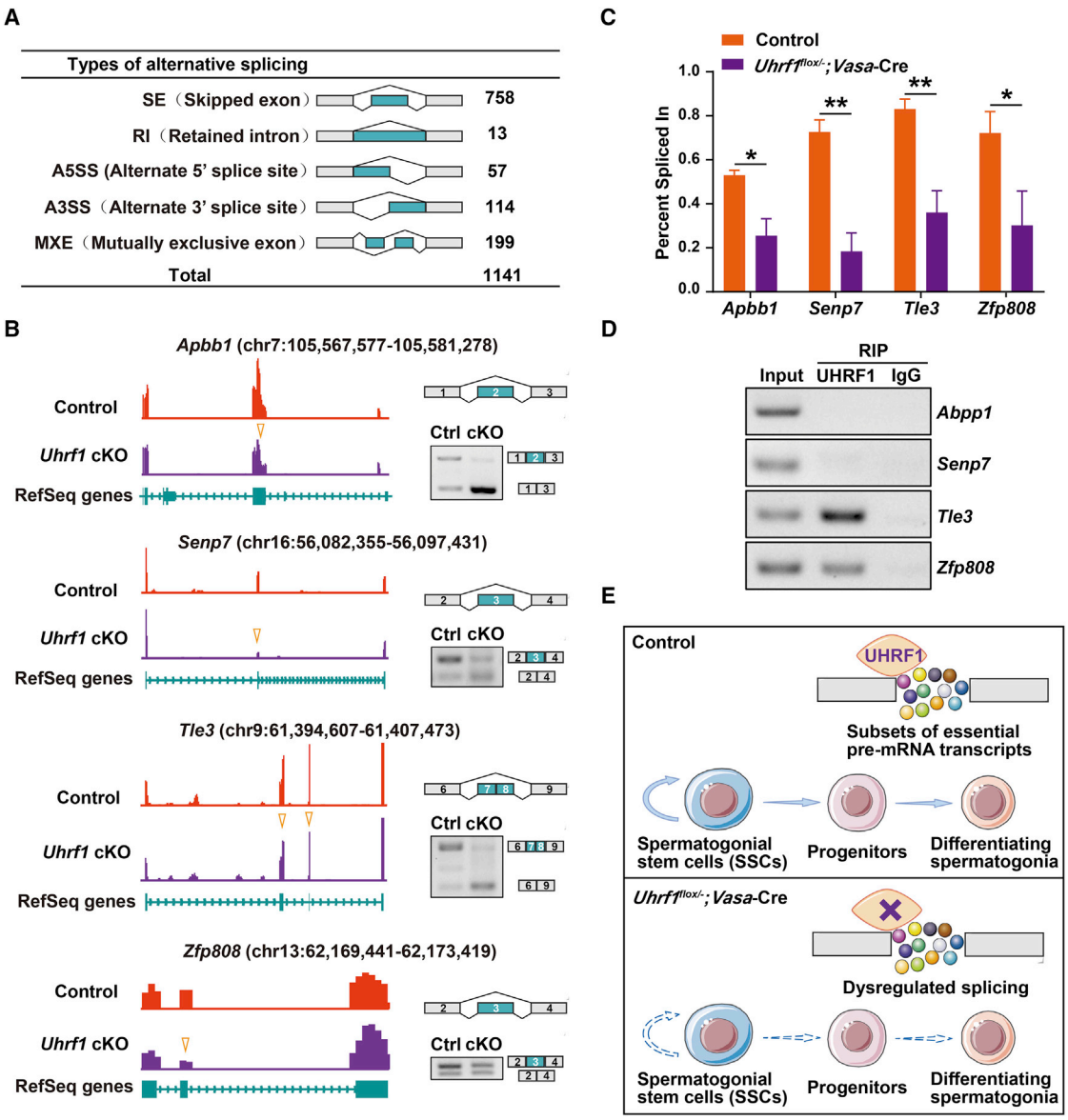

Figure 6. UHRF1 regulates alternative splicing in spermatogonia

(A) The differential alternative splicing events identified in *Uhrf1*$^{flox/-}$;*Vasa*-Cre testes at P7 are summarized. The numbers of individual alternative splicing events in each category upon UHRF1 ablation are indicated.

(B) Visualization of differential splicing analysis of RNA-sequencing data comparing control and *Uhrf1*$^{flox/-}$;*Vasa*-Cre testes at P7. (Left) Representative examples of a skipped exon (SE) in *Apbb1*, *Senp7*, *Tle3*, and *Zfp808*. (Right) RT-PCR validation of SEs by ethidium bromide-stained agarose gels.

(C) Bar chart shows the quantification of percentage spliced in (PSI); *p < 0.05, **p < 0.01.

(D) RNA immunoprecipitation (RIP) using UHRF1 antibody followed by PCR and gel electrophoresis for differentially spliced candidates (*Apbb1*, *Senp7*, *Tle3*, and *Zfp808*).

(E) A schematic model of UHRF1-mediated gene regulation in spermatogonia is shown. UHRF1 plays a critical role in post-transcriptional gene regulation. UHRF1 contributes to the fidelity of mRNA splicing in mouse spermatogonia.

DNA methylation and has been reported to preferentially interact with DNMT1 and bind to hemimethylated DNA, thereby tethering DNMT1 to newly replicated DNA and methylating the newly synthesized daughter strand (Achour et al., 2008; Bostick et al., 2007; Unoki et al., 2004). UHRF1 can also interact with DNMT3A and DNMT3B to regulate *de novo* DNA methylation in specific cellular contexts (Meilinger et al., 2009). In addition,

UHRF1 has been implicated in diverse aspects of histone modification, ranging from H3K9me2/3 to H3K4me0, H3R2me0, and H3 ubiquitination (Arita et al., 2012; Hu et al., 2011; Kim et al., 2009; Nishiyama et al., 2013; Qin et al., 2015; Rajakumara et al., 2011; Rothbart et al., 2012; Wang et al., 2011). Notably, previous studies found that AS of RNA can occur near chromosomes and is linked to histone modifications, complementing the traditional view of post-transcriptional AS and providing new clues for studying AS of pre-mRNA (Luco et al., 2011; Tilgner et al., 2012). Therefore, in the current study, we tried to decipher the biological function of UHRF1 in RNA AS. Indeed, our data revealed a novel role for UHRF1's function in spermatogonia that post-transcriptionally regulates pre-mRNA splicing, which adds another layer to UHRF1 in male germ cell development.

One of the intriguing findings in this study is that UHRF1 could interact with numerous RNA splicing factors. Of 337 candidate proteins interacting with UHRF1, up to 116 are associated with RNA splicing. These results suggest that, in addition to epigenetic regulation, UHRF1 is a unique RNA metabolic regulator in SSCs. In fact, consistent with the recent report of UHRF1 function in a cell line (Xu et al., 2021), we found that UHRF1 manifests a high binding intensity on U-rich snRNA, especially U1 snRNA, and interacts with both snRNPs and snRNAs in testes. In addition, the current study found that UHRF1 preferentially binds to U1, U2, and U4 snRNAs rather than U5 and U6 snRNAs; this binding preference suggests that UHRF1 may be involved in some specific processes during AS. Interestingly, in addition to the enrichment of 116 UHRF1-interacting proteins on the snRNP spliceosome, this study also found that some other co-immunoprecipitating proteins are enriched for the ribosome. On one hand, ribosome-directed pachytene piRNA formation is a breakthrough discovery that significantly enhances the theory of piRNA biogenesis (Sun et al., 2020, 2021). On the other hand, we previously showed that 25- to 32-bp reads of pachytene piRNAs were reduced by ~80% in *Uhrf1* cKO (*Stra8*-Cre induced) mice (Dong et al., 2019). Thus, combined with the finding in the current study that UHRF1 interacts with many ribosome proteins, it is highly likely that UHRF1 may function in ribosome-mediated piRNA biogenesis.

Further comparative RNA-seq data provide evidence that UHRF1 ablation leads to 1,141 aberrant AS events, supporting the function of UHRF1 as an RNA splicing regulator. In addition, we identified an intriguing gene, *Tle3*, on whose transcripts UHRF1 is enriched and regulates its exon skipping, suggesting that UHRF1 may bind to *Tle3* and thus contribute to its pre-mRNA splicing. Although *Tle3* has been reported to serve as an essential regulator in Sertoli cells and is highly expressed in spermatogonia, its role during spermatogenesis, especially in spermatogonia, is largely unknown (Lee et al., 2019). Given that we have demonstrated that UHRF1 affects the transcription of *Tle3* and binds to its mRNA to regulate AS, we speculate that *Tle3* is a critical downstream factor of UHRF1 and may shoulder the responsibility of SSC homeostasis. Moreover, this study confirmed that *Foxo1*, *Bcl6b*, and *Fgfr3* (three SSC homeostasis-related genes) (Goertz et al., 2011; Ishii et al., 2012; von Kopylow et al., 2010) were bound to UHRF1 by RIP-PCR, indicating that UHRF1 is directly associated with the transcripts related to spermatogonial maintenance. Given our data confirming the role of UHRF1 in pre-mRNA splicing and SSC homeostasis, we propose a model whereby UHRF1 supports the sustainable SSC pool by regulating gene-splicing programs (Figure 6E). However, considering that UHRF1 recruitment to pre-mRNA and regulation of AS have not appeared to be in the mainstream of scientific research in recent years (Newkirk and An, 2020; Xu et al., 2021), further study is required to confirm the significance of the UHRF1 RNA-binding function and identify in which conditions or in which tissues or cell types UHRF1 mediates RNA splicing.

In summary, our study provides new evidence of an essential role for UHRF1 in the self-renewal and differentiation of SSCs. Moreover, through a combination of IP/MS and RIP approaches, we confirmed UHRF1 as a newly identified AS factor that can bind to pre-mRNA and regulate AS. Overall, our study reveals new clues regarding the molecular mechanisms of UHRF1 that regulate SSC self-renewal and differentiation.

EXPERIMENTAL PROCEDURES

Mouse model generation

Uhrf1$^{flox/flox}$ mice were established in previous studies (Dong et al., 2019). *Vasa*-Cre mice were obtained from The Jackson Laboratory. Vasa-Cre males were first crossed with *Uhrf1*$^{flox/flox}$ females to generate the *Uhrf1*$^{+/flox}$;*Vasa*-Cre males, and then the *Uhrf1*$^{+/flox}$;*Vasa*-Cre male mice were bred with *Uhrf1*$^{flox/flox}$ female mice to obtain the *Uhrf1*$^{flox/-}$;*Vasa*-Cre (designated *Uhrf1* cKO) males. Mice were housed in a barrier facility at the Institutional Animal Care and Use Committee of Huazhong University of Science and Technology. All experimental procedures were conducted ethically according to ethical requirements and approved by the Institutional Animal Care and Use Committee of Huazhong University of Science and Technology, Wuhan, Hubei. Mice were genotyped with specific primer sets (Table S6).

Fertility test assay

To assess fertility, pairs of *Uhrf1*$^{flox/-}$;*Vasa*-Cre, *Uhrf1*$^{+/flox}$;*Vasa*-Cre, and *Uhrf1* $^{flox/flox}$ female mice were co-caged with *Uhrf1*$^{flox/-}$;*Vasa*-Cre, *Uhrf1*$^{+/flox}$;*Vasa*-Cre, or *Uhrf1* $^{flox/flox}$ male mice for 6 months.

The average number of pups per litter was quantified and at least three mating cages were set up for each genotype.

Histological analysis

Testes and epididymides were fixed in Bouin's solution (Sigma, HT10132) at 4°C overnight and then washed with 75% alcohol four to six times. Samples were then embedded in paraffin, sectioned (5 μm thick), and mounted on slides before staining with periodic acid-Schiff (PAS).

Immunofluorescence

Immunofluorescence was performed on cryosections of testes. Briefly, testes were fixed in 4% paraformaldehyde (Sigma), dehydrated in sucrose (Sigma), embedded in OCT (Sakura Finetek, 4583) and sectioned (5 μm thick). After antigen retrieval with 0.01% sodium citrate buffer (pH 6.0), the sections were blocked in blocking solution (5% donkey serum in PBS) for 1 h and incubated with primary antibodies (Table S6) overnight at 4°C. Then, the secondary antibodies conjugated to Alexa Fluor were used to detect the antigen, and VECTASHIELD mounting medium containing DAPI (H1200, Vector Laboratories) was used to mount slides. Cell apoptosis was measured by TUNEL assay using an *In Situ* Cell Death Detection kit, fluorescein (Roche), according to the manufacturer's instructions. Laser confocal scanning images were captured using an Axio Scope A1 fluorescence microscope (Zeiss, Germany) with a digital camera (MSX2, Microshot Technology, China).

Western blotting

Total protein was extracted in RIPA buffer (CWBIO, cat. No. 01408). Proteins were separated on 8%–12% Bis-Tris gels and transferred to polyvinylidene difluoride (PVDF) membranes (Bio-Rad). The membranes were blocked with 5% non-fat dry milk (Bio-Rad) in Tris-buffered saline containing 0.01% Tween 20 (TBST) at room temperature (RT) for 1 h and probed with primary antibodies (Table S6) overnight at 4°C. The membranes were then washed three times with TBST and incubated (1–2 h, RT) with secondary antibodies (Table S6), washed with TBST, and developed using Luminol/enhancer solution and peroxide solution (Clarity Western ECL Substrate, Bio-Rad) according to the manufacturer's instructions.

RNA isolation and quantitative real-time RT-PCR

Total RNA was isolated from mouse tissues using TRIzol reagent (Invitrogen, 15596-025) following the manufacturer's procedure, and cDNA was synthesized with a PrimeScript RT reagent kit with gDNA Eraser (TaKaRa) to remove DNA contamination. For RNA isolation for RIP experiments, a slightly modified RNA extraction procedure based on the standard manufacturer's protocol was used to promote the precipitation of RNA and U snRNA. In the RNA precipitation procedure, RNA was precipitated with 2.5–3.0 volumes of ethanol (Sigma-Aldrich, E7023) in the presence of 0.5 M ammonium acetate (Invitrogen, AM9070G) and 100 μg/mL glycogen (Invitrogen, AM9510) at −20°C overnight. RNA (0.5–1 μg) was reverse synthesized with a PrimeScript RT reagent kit with gDNA Eraser (TaKaRa, RR047) following the manufacturer's protocol. Quantitative RT-PCR was performed using SYBR green master mix (YEASEN, 11201ES03) in a Step One ABI real-time PCR system according to the manufacturer's instructions. The primers used in these experiments are listed in Table S6. For RT-PCR, the relative abundance of each transcript was calculated by the $2^{-\Delta\Delta Ct}$ method normalized to the GAPDH expression. For RIP-PCR, enrichment of RNA is shown as the percentage input, which was calculated by determining the apparent immunoprecipitation efficiency at the indicated loci as the ratio of the amount of immunoprecipitated RNA to the normalized amount of starting material (percentage of input RNA).

RNA-seq analysis

Total RNA was isolated from P0 and P7 mouse testes (three biological repeats each for control and *Vasa*-Cre;*Uhrf1*$^{flox/-}$) using TRIzol reagent (Invitrogen). The RNA concentration was verified using a NanoDrop 2000 spectrophotometer (Thermo Fisher Scientific). One microgram of total RNA was used from each sample to prepare mRNA libraries using TruSeq Stranded mRNA Library Preparation Kit Set A (cat. no. RS-122-2101; Illumina) according to the manufacturer's instructions. All libraries were sequenced using the Illumina HiSeq 4000 platform. The FASTX-Toolkit was used to remove adaptor sequences and low-quality reads from the sequencing data. To identify all the transcripts, we used Tophat2 and Cufflinks to assemble the sequencing reads based on the UCSC MM10 mouse genome. The differential expression analysis was performed by DESeq2. The differentially expressed genes were set with the threshold of $p < 0.05$ and fold change ≥ 2.

Differential splicing analysis was performed using rMATS. To detect valid AS events, those with FDR < 0.05 and $|\Delta\psi| > 0.05$ were categorized as differential AS events, which were classified into five types, known as skipped exon (SE), alternative 5′ splice site (A5SS), alternative 3′ splice site (A3SS), mutually exclusive exons (MXEs), and retained intron (RI). The genes of differential AS events were used for GO enrichment analysis through Metascape (Zhou et al., 2019).

Isolation of SSCs by MACS

Testes from pups on P6–P8 were dissected, decapsulated, and washed with ice-cold HBSS. Then the testicular tissues were digested in collagenase solution (1 mg/mL collagenase IV and 1 mg/mL DNase I in HBSS). After digestion at 37°C on a shaker for 15 min, the seminiferous tubules were allowed to settle and were subsequently washed twice with E-HBSS (2 mM EDTA in HBSS). After centrifugation (100*g*), the precipitates were collected and incubated in trypsin solution (1 mg/mL DNase I in 0.25% trypsin-EDTA) for 3–5 min at 37°C. Afterward, the trypsin reaction was quenched by adding F-MACS (10% FBS in MACS buffer), and the suspension was filtered with 70 μm pore-size nylon mesh. The filtered solution was collected in a 15 mL sterile centrifuge tube and centrifuged at 600*g*/min for 5 min. The dissociated cells were collected after washing once with 2-fold volumes of MACS buffer. Then the testicular cells were resuspended in 100 μL ice-cold MACS buffer supplemented with anti-CD90.2 (THY1) microbeads (Miltenyi Biotec, 130-121-278). After incubation at 4°C for 15 min, THY1$^+$ spermatogonia were purified by a MiniMACS starting kit (Miltenyi Biotec, 130-090-312) according

to the manufacturer's instructions and stored at −80°C for the experiments.

Co-immunoprecipitation and mass spectrometry

Lysates from freshly isolated SSCs were prepared using immunoprecipitation buffer (Beyotime), placed on a rotary shaker for 30 min, and then clarified by centrifugation at 12,000*g*. UHRF1 complexes were immunoprecipitated with rabbit anti-UHRF1 (Proteintech, 21402-1-AP) coupled with protein A beads (Bio-Rad, 161-4013) according to the manufacturer's instructions. Elution and preparation of samples for mass spectrometry analysis were performed as described previously at the Bio21 Proteomics Facility (Chan et al., 2017). GO analysis was performed on mass spectrometry data using Metascape (Zhou et al., 2019).

RNA immunoprecipitation

Isolated spermatogonia were used for all RIP experiments. The spermatogonia were digested in lysis buffer (50 mM Tris [pH 8], 150 mM NaCl, 0.5% sodium deoxycholate, 1% Triton X-100, 5 mM $MgCl_2$, 1 mM DTT, 1/50 protease inhibitor cocktail, 2 mM RVC RNase inhibitor) and placed on a rotary shaker for 30 min. The lysates were collected, centrifuged at 12,000*g*, and incubated with anti-UHRF1 (Proteintech, 21402-1-AP) antibodies overnight at 4°C on a rotator. Then, protein A beads (Bio-Rad, 161-4013) were added to the lysates for a 4 h incubation after being washed with lysis buffer. Following this incubation, the beads were washed with high-salt buffer (5 mM $MgCl_2$, 1 mM DTT, 1/50 protease inhibitor cocktail, 2 mM RVC RNase inhibitor) two times and wash buffer (20 mM Tris [pH 8], 150 mM NaCl, 0.5% NP-40) three times for the RNA extraction assay.

Statistical analysis

Unless otherwise noted, data are presented as the mean ± SEM. The two-tailed Student t test was used to calculate p values, and $p < 0.05$ was considered statistically significant.

Data and code availability

All RNA sequencing data reported in this study are deposited in the NCBI Sequence Read Achieve (SRA) database. The accession number for the sequence data reported in this paper is SRA: SRP356228. Previously published and available scRNA-seq data were used for Figures 1 and S1 with accession code GSE152930 (Hermann et al., 2018). All other relevant data that support the findings of this study are available from the corresponding authors upon reasonable request.

SUPPLEMENTAL INFORMATION

Supplemental information can be found online at https://doi.org/10.1016/j.stemcr.2022.06.010.

AUTHOR CONTRIBUTIONS

S.Y. and Y.G. conceived and designed the research. S.Z. and J.D. performed the experiments. M.X., Y.W., J.Z., and X.W. provided methodological guidance. S.Z. and S.G. performed RNA-seq library construction and bioinformatics analysis. S.Z. and S.Y. wrote the paper. S.Y. supervised the project.

ACKNOWLEDGMENTS

We are grateful to the members of the Yuan laboratory for discussion in the very initial phase of the project. This work was supported in part by grants from the National Natural Science Foundation of China (82171605 and 81971444 to S.Y.), the Science Technology and Innovation Commission of Shenzhen Municipality (JCYJ20170818160910316 to S.Y.), and the foundation of Guangdong Key Laboratory of Male Reproductive Medicine and Genetics (PKUSZH2021001 and PKUSZH2021002).

CONFLICTS OF INTERESTS

The authors declare no competing interests.

Received: January 27, 2022
Revised: June 27, 2022
Accepted: June 28, 2022
Published: July 28, 2022

REFERENCES

Achour, M., Jacq, X., Rondé, P., Alhosin, M., Charlot, C., Chataigneau, T., Jeanblanc, M., Macaluso, M., Giordano, A., Hughes, A.D., et al. (2008). The interaction of the SRA domain of ICBP90 with a novel domain of DNMT1 is involved in the regulation of VEGF gene expression. Oncogene *27*, 2187–2197. https://doi.org/10.1038/sj.onc.1210855.

Arita, K., Isogai, S., Oda, T., Unoki, M., Sugita, K., Sekiyama, N., Kuwata, K., Hamamoto, R., Tochio, H., Sato, M., et al. (2012). Recognition of modification status on a histone H3 tail by linked histone reader modules of the epigenetic regulator UHRF1. Proc. Natl. Acad. Sci. USA *109*, 12950–12955. https://doi.org/10.1073/pnas.1203701109.

Baralle, F.E., and Giudice, J. (2017). Alternative splicing as a regulator of development and tissue identity. Nat. Rev. Mol. Cell Biol. *18*, 437–451. https://doi.org/10.1038/nrm.2017.27.

Bostick, M., Kim, J.K., Esteve, P.O., Clark, A., Pradhan, S., and Jacobsen, S.E. (2007). UHRF1 plays a role in maintaining DNA methylation in mammalian cells. Science *317*, 1760–1764. https://doi.org/10.1126/science.1147939.

Cao, Y., Li, M., Liu, F., Ni, X., Wang, S., Zhang, H., Sui, X., and Huo, R. (2019). Deletion of maternal UHRF1 severely reduces mouse oocyte quality and causes developmental defects in preimplantation embryos. FASEB J. *33*, 8294–8305. https://doi.org/10.1096/fj.201801696RRRR.

Chan, A.L., La, H.M., Legrand, J.M., Mäkelä, J.A., Eichenlaub, M., De Seram, M., Ramialison, M., and Hobbs, R.M. (2017). Germline stem cell activity is sustained by SALL4-dependent silencing of distinct tumor suppressor genes. Stem Cell Rep. *9*, 956–971. https://doi.org/10.1016/j.stemcr.2017.08.001.

Chen, H., Ma, H., Inuzuka, H., Diao, J., Lan, F., Shi, Y.G., Wei, W., and Shi, Y. (2013). DNA damage regulates UHRF1 stability via the SCF(β-TrCP) E3 ligase. Mol. Cell Biol. *33*, 1139–1148. https://doi.org/10.1128/mcb.01191-12.

de Rooij, D.G. (2017). The nature and dynamics of spermatogonial stem cells. Development *144*, 3022–3030. https://doi.org/10.1242/dev.146571.

Dominguez, D., Tsai, Y.H., Weatheritt, R., Wang, Y., Blencowe, B.J., and Wang, Z. (2016). An extensive program of periodic alternative splicing linked to cell cycle progression. Elife *5*, e10288. https://doi.org/10.7554/eLife.10288.

Dong, J., Wang, X., Cao, C., Wen, Y., Sakashita, A., Chen, S., Zhang, J., Zhang, Y., Zhou, L., Luo, M., et al. (2019). UHRF1 suppresses retrotransposons and cooperates with PRMT5 and PIWI proteins in male germ cells. Nat. Commun. *10*, 4705. https://doi.org/10.1038/s41467-019-12455-4.

Fujimori, A., Matsuda, Y., Takemoto, Y., Hashimoto, Y., Kubo, E., Araki, R., Fukumura, R., Mita, K., Tatsumi, K., and Muto, M. (1998). Cloning and mapping of Np95 gene which encodes a novel nuclear protein associated with cell proliferation. Mamm. Genome *9*, 1032–1035. https://doi.org/10.1007/s003359900920.

Goertz, M.J., Wu, Z., Gallardo, T.D., Hamra, F.K., and Castrillon, D.H. (2011). Foxo1 is required in mouse spermatogonial stem cells for their maintenance and the initiation of spermatogenesis. J. Clin. Invest. *121*, 3456–3466. https://doi.org/10.1172/JCI57984.

Hermann, B.P., Cheng, K., Singh, A., Roa-De La Cruz, L., Mutoji, K.N., Chen, I.C., Gildersleeve, H., Lehle, J.D., Mayo, M., Westernströer, B., et al. (2018). The mammalian spermatogenesis single-cell transcriptome, from spermatogonial stem cells to spermatids. Cell Rep. *25*, 1650–1667.e8. https://doi.org/10.1016/j.celrep.2018.10.026.

Hopfner, R., Mousli, M., Jeltsch, J.M., VoulgAris, A., Lutz, Y., Marin, C., Bellocq, J.P., Oudet, P., Bronner, C., and VoulgAris, A. (2000). ICBP90, a novel human CCAAT binding protein, involved in the regulation of topoisomerase IIalpha expression. Cancer Res. *60*, 121–128.

Hu, L., Li, Z., Wang, P., Lin, Y., and Xu, Y. (2011). Crystal structure of PHD domain of UHRF1 and insights into recognition of unmodified histone H3 arginine residue 2. Cell Res. *21*, 1374–1378. https://doi.org/10.1038/cr.2011.124.

Ishii, K., Kanatsu-Shinohara, M., Toyokuni, S., and Shinohara, T. (2012). FGF2 mediates mouse spermatogonial stem cell self-renewal via upregulation of Etv5 and Bcl6b through MAP2K1 activation. Development *139*, 1734–1743. https://doi.org/10.1242/dev.076539.

Kim, J.K., Estève, P.O., Jacobsen, S.E., and Pradhan, S. (2009). UHRF1 binds G9a and participates in p21 transcriptional regulation in mammalian cells. Nucleic Acids Res. *37*, 493–505. https://doi.org/10.1093/nar/gkn961.

La, H.M., Chan, A.L., Legrand, J.M.D., Rossello, F.J., Gangemi, C.G., Papa, A., Cheng, Q., Morand, E.F., and Hobbs, R.M. (2018). GILZ-dependent modulation of mTORC1 regulates spermatogonial maintenance. Development *145*, dev165324. https://doi.org/10.1242/dev.165324.

Lee, S., Jang, H., Moon, S., Lee, O.H., Lee, S., Lee, J., Park, C., Seol, D.W., Song, H., Hong, K., et al. (2019). Differential regulation of TLE3 in Sertoli cells of the testes during postnatal development. Cells *8*, 1156. https://doi.org/10.3390/cells8101156.

Legrand, J.M., and Hobbs, R.M. (2018). RNA processing in the male germline: mechanisms and implications for fertility. Semin. Cell Dev. Biol. *79*, 80–91. https://doi.org/10.1016/j.semcdb.2017.10.006.

Legrand, J.M.D., Chan, A.L., La, H.M., Rossello, F.J., Änkö, M.L., Fuller-Pace, F.V., and Hobbs, R.M. (2019). DDX5 plays essential transcriptional and post-transcriptional roles in the maintenance and function of spermatogonia. Nat. Commun. *10*, 2278. https://doi.org/10.1038/s41467-019-09972-7.

Liu, W., Wang, F., Xu, Q., Shi, J., Zhang, X., Lu, X., Zhao, Z.A., Gao, Z., Ma, H., Duan, E., et al. (2017). BCAS2 is involved in alternative mRNA splicing in spermatogonia and the transition to meiosis. Nat. Commun. *8*, 14182. https://doi.org/10.1038/ncomms14182.

Luco, R.F., Allo, M., Schor, I.E., Kornblihtt, A.R., and Misteli, T. (2011). Epigenetics in alternative pre-mRNA splicing. Cell *144*, 16–26. https://doi.org/10.1016/j.cell.2010.11.056.

Meilinger, D., Fellinger, K., Bultmann, S., Rothbauer, U., Bonapace, I.M., Klinkert, W.E.F., Spada, F., and Leonhardt, H. (2009). Np95 interacts with de novo DNA methyltransferases, Dnmt3a and Dnmt3b, and mediates epigenetic silencing of the viral CMV promoter in embryonic stem cells. EMBO Rep. *10*, 1259–1264. https://doi.org/10.1038/embor.2009.201.

Muto, M., Kanari, Y., Kubo, E., Takabe, T., Kurihara, T., Fujimori, A., and Tatsumi, K. (2002). Targeted disruption of Np95 gene renders murine embryonic stem cells hypersensitive to DNA damaging agents and DNA replication blocks. J. Biol. Chem. *277*, 34549–34555. https://doi.org/10.1074/jbc.M205189200.

Muto, M., Fujimori, A., Nenoi, M., Daino, K., Matsuda, Y., Kuroiwa, A., Kubo, E., Kanari, Y., Utsuno, M., Tsuji, H., et al. (2006). Isolation and characterization of a novel human radiosusceptibility gene, NP95. Radiat. Res. *166*, 723–733. https://doi.org/10.1667/rr0459.1.

Nakagawa, T., Sharma, M., Nabeshima, Y.i., Braun, R.E., and Yoshida, S. (2010). Functional hierarchy and reversibility within the murine spermatogenic stem cell compartment. Science *328*, 62–67. https://doi.org/10.1126/science.1182868.

Newkirk, S.J., and An, W. (2020). UHRF1: a jack of all trades, and a master epigenetic regulator during spermatogenesis. Biol. Reprod. *102*, 1147–1152. https://doi.org/10.1093/biolre/ioaa026.

Nilsen, T.W., and Graveley, B.R. (2010). Expansion of the eukaryotic proteome by alternative splicing. Nature *463*, 457–463. https://doi.org/10.1038/nature08909.

Nishiyama, A., Yamaguchi, L., Sharif, J., Johmura, Y., Kawamura, T., Nakanishi, K., Shimamura, S., Arita, K., Kodama, T., Ishikawa, F., et al. (2013). Uhrf1-dependent H3K23 ubiquitylation couples maintenance DNA methylation and replication. Nature *502*, 249–253. https://doi.org/10.1038/nature12488.

Oltean, S., and Bates, D.O. (2014). Hallmarks of alternative splicing in cancer. Oncogene *33*, 5311–5318. https://doi.org/10.1038/onc.2013.533.

Pan, H., Jiang, N., Sun, S., Jiang, H., Xu, J., Jiang, X., Gao, Q., Li, L., Wu, H., Zheng, H., et al. (2020). UHRF1-repressed 5′-hydroxymethylcytosine is essential for the male meiotic prophase I. Cell Death Dis. *11*, 142. https://doi.org/10.1038/s41419-020-2333-3.

Qin, W., Wolf, P., Liu, N., Link, S., Smets, M., Mastra, F.L., Forné, I., Pichler, G., Hörl, D., Fellinger, K., et al. (2015). DNA methylation requires a DNMT1 ubiquitin interacting motif (UIM) and histone ubiquitination. Cell Res. *25*, 911–929. https://doi.org/10.1038/cr.2015.72.

Rajakumara, E., Wang, Z., Ma, H., Hu, L., Chen, H., Lin, Y., Guo, R., Wu, F., Li, H., Lan, F., et al. (2011). PHD finger recognition of unmodified histone H3R2 links UHRF1 to regulation of euchromatic gene expression. Mol. Cell *43*, 275–284. https://doi.org/10.1016/j.molcel.2011.07.006.

Rothbart, S.B., Krajewski, K., Nady, N., Tempel, W., Xue, S., Badeaux, A.I., Barsyte-Lovejoy, D., Martinez, J.Y., Bedford, M.T., Fuchs, S.M., et al. (2012). Association of UHRF1 with methylated H3K9 directs the maintenance of DNA methylation. Nat. Struct. Mol. Biol. *19*, 1155–1160. https://doi.org/10.1038/nsmb.2391.

Sun, Y.H., Zhu, J., Xie, L.H., Li, Z., Meduri, R., Zhu, X., Song, C., Chen, C., Ricci, E.P., Weng, Z., and Li, X.Z. (2020). Ribosomes guide pachytene piRNA formation on long intergenic piRNA precursors. Nat. Cell Biol. *22*, 200–212. https://doi.org/10.1038/s41556-019-0457-4.

Sun, Y.H., Wang, R.H., Du, K., Zhu, J., Zheng, J., Xie, L.H., Pereira, A.A., Zhang, C., Ricci, E.P., and Li, X.Z. (2021). Coupled protein synthesis and ribosome-guided piRNA processing on mRNAs. Nat. Commun. *12*, 5970. https://doi.org/10.1038/s41467-021-26233-8.

Takada, Y., Yaman-Deveci, R., Shirakawa, T., Sharif, J., Tomizawa, S.I., Miura, F., Ito, T., Ono, M., Nakajima, K., Koseki, Y., et al. (2021). Maintenance DNA methylation in pre-meiotic germ cells regulates meiotic prophase by facilitating homologous chromosome pairing. Development *148*, dev194605. https://doi.org/10.1242/dev.194605.

Tien, A., Senbanerjee, S., Kulkarni, A., Mudbhary, R., Goudreau, B., Ganesan, S., Sadler, K., and Ukomadu, C. (2011). UHRF1 depletion causes a G2/M arrest, activation of DNA damage response and apoptosis. Biochem. J. *435*, 175–185. https://doi.org/10.1042/bj20100840.

Tilgner, H., Knowles, D.G., Johnson, R., Davis, C.A., Chakrabortty, S., Djebali, S., Curado, J., Snyder, M., Gingeras, T.R., and Guigó, R. (2012). Deep sequencing of subcellular RNA fractions shows splicing to be predominantly co-transcriptional in the human genome but inefficient for lncRNAs. Genome Res. *22*, 1616–1625. https://doi.org/10.1101/gr.134445.111.

Ule, J., and Blencowe, B.J. (2019). Alternative splicing regulatory networks: functions, mechanisms, and evolution. Mol. Cell *76*, 329–345. https://doi.org/10.1016/j.molcel.2019.09.017.

Unoki, M., Nishidate, T., and Nakamura, Y. (2004). ICBP90, an E2F-1 target, recruits HDAC1 and binds to methyl-CpG through its SRA domain. Oncogene *23*, 7601–7610. https://doi.org/10.1038/sj.onc.1208053.

von Kopylow, K., Kirchhoff, C., Jezek, D., Schulze, W., Feig, C., Primig, M., Steinkraus, V., and Spiess, A.N. (2010). Screening for biomarkers of spermatogonia within the human testis: a whole genome approach. Hum. Reprod. *25*, 1104–1112. https://doi.org/10.1093/humrep/deq053.

Wang, E.T., Sandberg, R., Luo, S., Khrebtukova, I., Zhang, L., Mayr, C., Kingsmore, S.F., Schroth, G.P., and Burge, C.B. (2008). Alternative isoform regulation in human tissue transcriptomes. Nature *456*, 470–476. https://doi.org/10.1038/nature07509.

Wang, C., Shen, J., Yang, Z., Chen, P., Zhao, B., Hu, W., Lan, W., Tong, X., Wu, H., Li, G., and Cao, C. (2011). Structural basis for site-specific reading of unmodified R2 of histone H3 tail by UHRF1 PHD finger. Cell Res. *21*, 1379–1382. https://doi.org/10.1038/cr.2011.123.

Wang, Z., Xu, X., Li, J.L., Palmer, C., Maric, D., and Dean, J. (2019). Sertoli cell-only phenotype and scRNA-seq define PRAMEF12 as a factor essential for spermatogenesis in mice. Nat. Commun. *10*, 5196. https://doi.org/10.1038/s41467-019-13193-3.

Wu, Y., Dong, J., Feng, S., Zhao, Q., Duan, P., Xiong, M., Wen, Y., Lv, C., Wang, X., and Yuan, S. (2020). Maternal UHRF1 is essential for transcription landscapes and repression of repetitive elements during the maternal-to-zygotic transition. Front. Cell Dev. Biol. *8*, 610773. https://doi.org/10.3389/fcell.2020.610773.

Xu, P., Zhang, L., Xiao, Y., Li, W., Hu, Z., Zhang, R., Li, J., Wu, F., Xi, Y., Zou, Q., et al. (2021). UHRF1 regulates alternative splicing by interacting with splicing factors and U snRNAs in a H3R2me involved manner. Hum. Mol. Genet. *30*, 2110–2122. https://doi.org/10.1093/hmg/ddab178.

Yamaji, M., Jishage, M., Meyer, C., Suryawanshi, H., Der, E., Yamaji, M., Garzia, A., Morozov, P., Manickavel, S., McFarland, H.L., et al. (2017). DND1 maintains germline stem cells via recruitment of the CCR4-NOT complex to target mRNAs. Nature *543*, 568–572. https://doi.org/10.1038/nature21690.

Zhou, Z., Shirakawa, T., Ohbo, K., Sada, A., Wu, Q., Hasegawa, K., Saba, R., and Saga, Y. (2015). RNA binding protein Nanos2 organizes post-transcriptional buffering system to retain primitive state of mouse spermatogonial stem cells. Dev. Cell *34*, 96–107. https://doi.org/10.1016/j.devcel.2015.05.014.

Zhou, Y., Zhou, B., Pache, L., Chang, M., Khodabakhshi, A.H., Tanaseichuk, O., Benner, C., and Chanda, S.K. (2019). Metascape provides a biologist-oriented resource for the analysis of systems-level datasets. Nat. Commun. *10*, 1523. https://doi.org/10.1038/s41467-019-09234-6.

Zhou, S., Feng, S., Qin, W., Wang, X., Tang, Y., and Yuan, S. (2021). Epigenetic regulation of spermatogonial stem cell homeostasis: from DNA methylation to histone modification. Stem Cell Rev. Rep. *17*, 562–580. https://doi.org/10.1007/s12015-020-10044-3.

Stem Cell Reports, Volume *17*

Supplemental Information

UHRF1 interacts with snRNAs and regulates alternative splicing in mouse spermatogonial stem cells

Shumin Zhou, Juan Dong, Mengneng Xiong, Shiming Gan, Yujiao Wen, Jin Zhang, Xiaoli Wang, Shuiqiao Yuan, and Yaoting Gui

Supplemental Information

UHRF1 interacts with snRNAs and regulates alternative splicing in mouse spermatogonial stem cells

Shumin Zhou, Juan Dong, Mengneng Xiong, Shiming Gan, Yujiao Wen, Jin Zhang, Xiaoli Wang, Shuiqiao Yuan, Yaoting Gui

Supplemental Figures

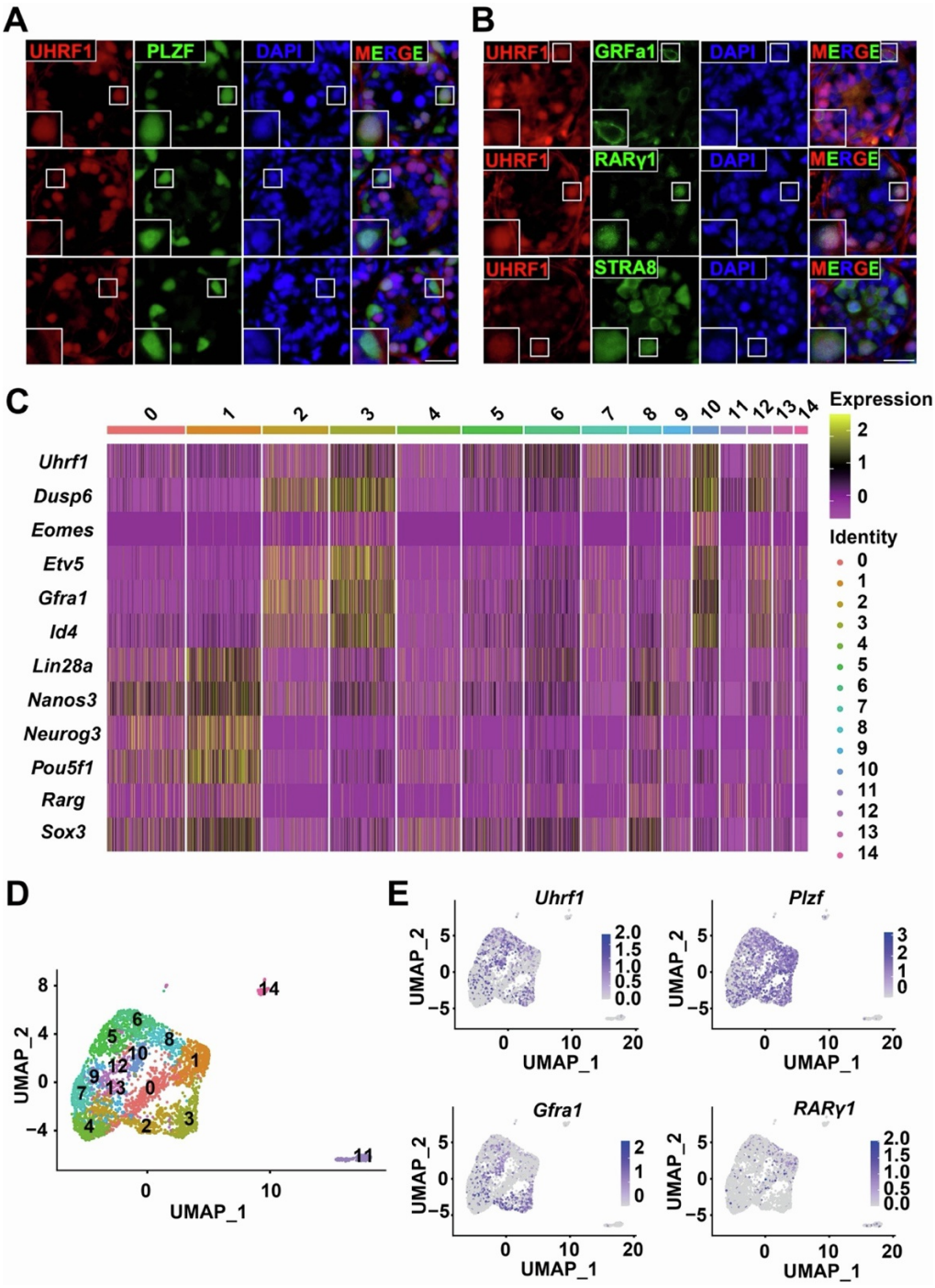

Figure S1. UHRF1 manifests a dynamic expression profile in undifferentiated spermatogonia.

(A) Double immunostaining of PLZF (green) and UHRF1(red) reveals a high, modest, and weak UHRF1 signal in PLZF-positive spermatogonia. Scale bar =25 μm.

(B) Mouse seminiferous tubule immunofluorescence showing expression of UHRF1 in stem/self-renewing (GFRα1-positive), progenitor (RARγ1-positive), and differentiating (STRA8-positive) spermatogonia populations. Scale bar =25 μm.

(C) Heatmap analysis of the published scRNA-seq data showing the expression pattern of *Uhrf1* and 11 spermatogonial marker genes. The color key from purple to bright yellow indicates low to high gene expression levels.

(D-E) Expression patterns of *Uhrf1* and selective marker genes of undifferentiated spermaotogonia, spermatogonial stem cells, progenitor spermatogonia were visualized by tSNE plots of scRNA-seq.

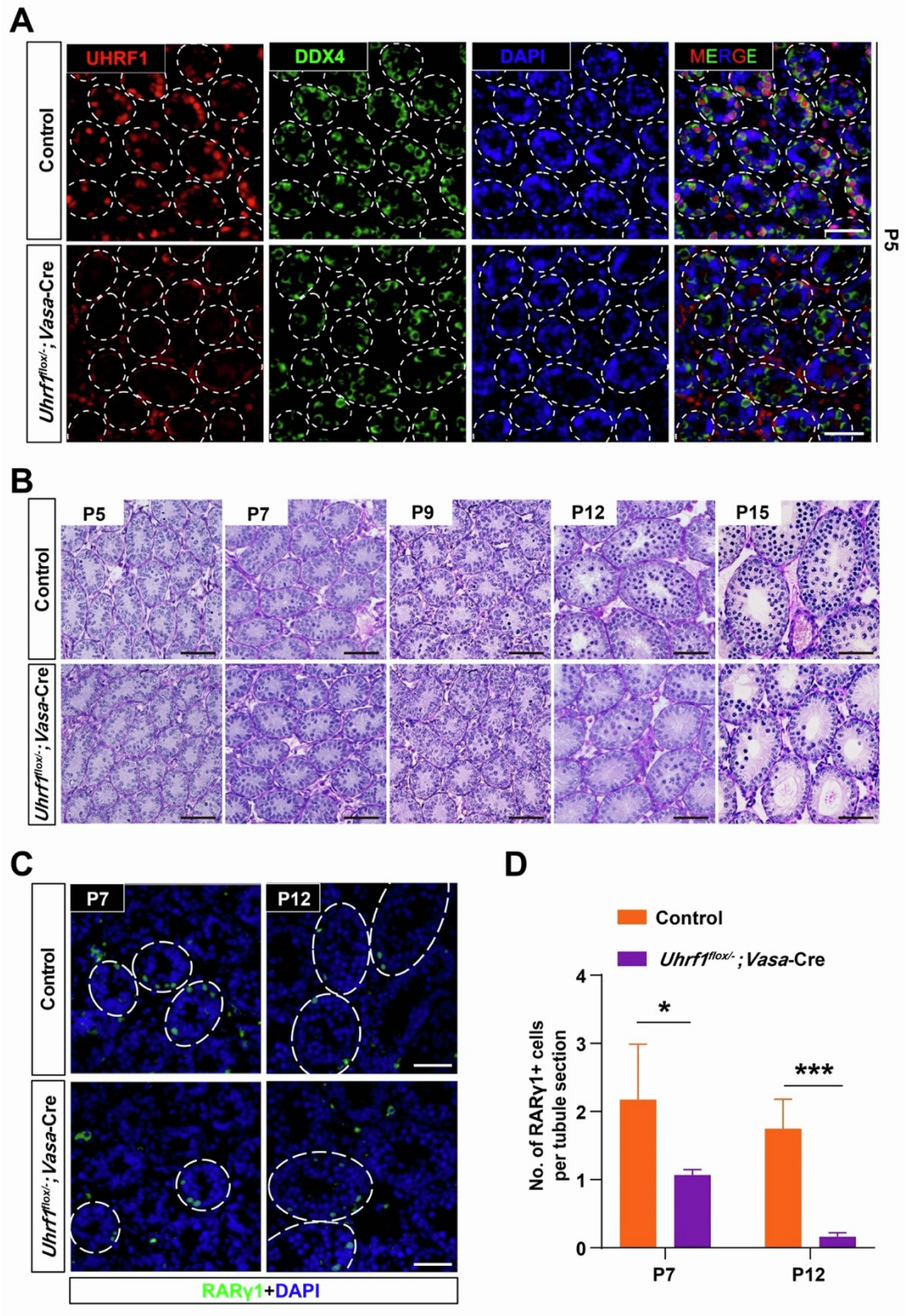

Figure S2. UHRF1 ablation causes progenitor spermatogonial populations to decrease.

(A) Co-immunofluorescent staining for the UHRF1 (red) and DDX4 (green) on control and *Uhrf1*$^{flox/-}$;*Vasa*-Cre testis sections at P5. Scale bars = 50 μm.

(B) Periodic acid-Schiff (PAS) staining of testis sections from *Uhrf1*$^{flox/-}$; *Vasa*-Cre and control mice at P5, P7, P9, P12, and P15. Scale bars = 50 μm.

(C) Immunofluorescence images of seminiferous tubules at P7 and P12 stained for RARγ1 (green).

(D) Quantification of the number of RARγ1-positive cells per tubule for (C). Data are presented as mean ± SEM. n = 3. *P <0.05, ***P < 0.001.

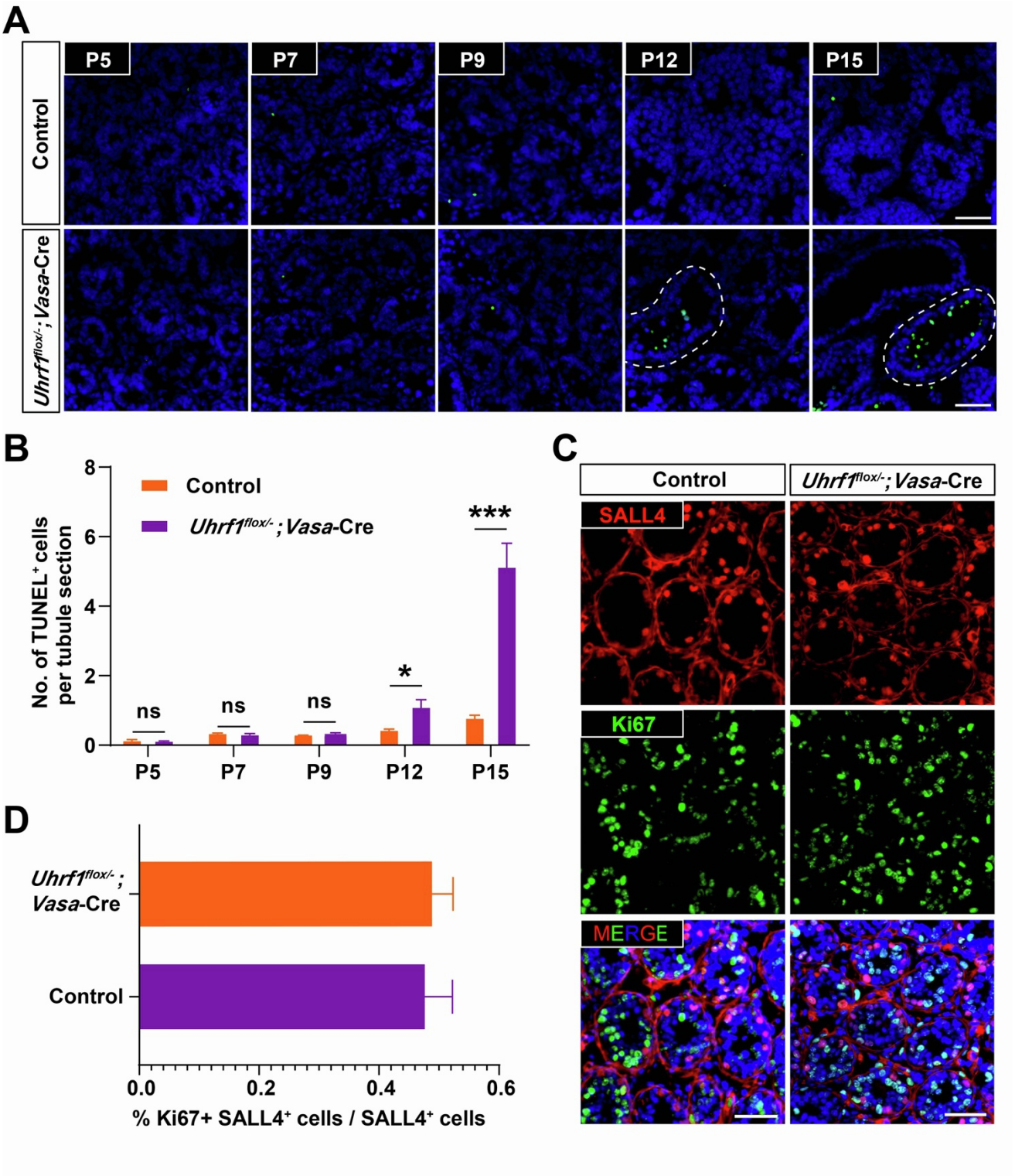

Figure S3. UHRF1 is dispensable for the proliferation and apoptosis of undifferentiated spermatogonia.

(A) Representative TUNEL staining images of testicular sections from control and *Uhrf1*$^{flox/-}$;*Vasa*-Cre mice at P5, P7, P9, P12, and P15. Nuclei are counterstained with DAPI (DNA). Scale bars = 50 μm.

(B) Quantification of the number of apoptotic cells per tubule for (A). Data are presented as mean ± SEM. n = 3. *P <0.05, ***P < 0.001.

(C) Co-immunofluorescent staining for the SALL4 (red) and Ki67 (green) on control and *Uhrf1*$^{flox/-}$;*Vasa*-Cre testis sections at P7. Scale bars = 50 μm.

(D) Graph showing the percent of Ki67$^+$ SALL4$^+$ cells in the SALL4$^+$ population clone types for (C). Data are presented as mean ± SEM. n = 3.

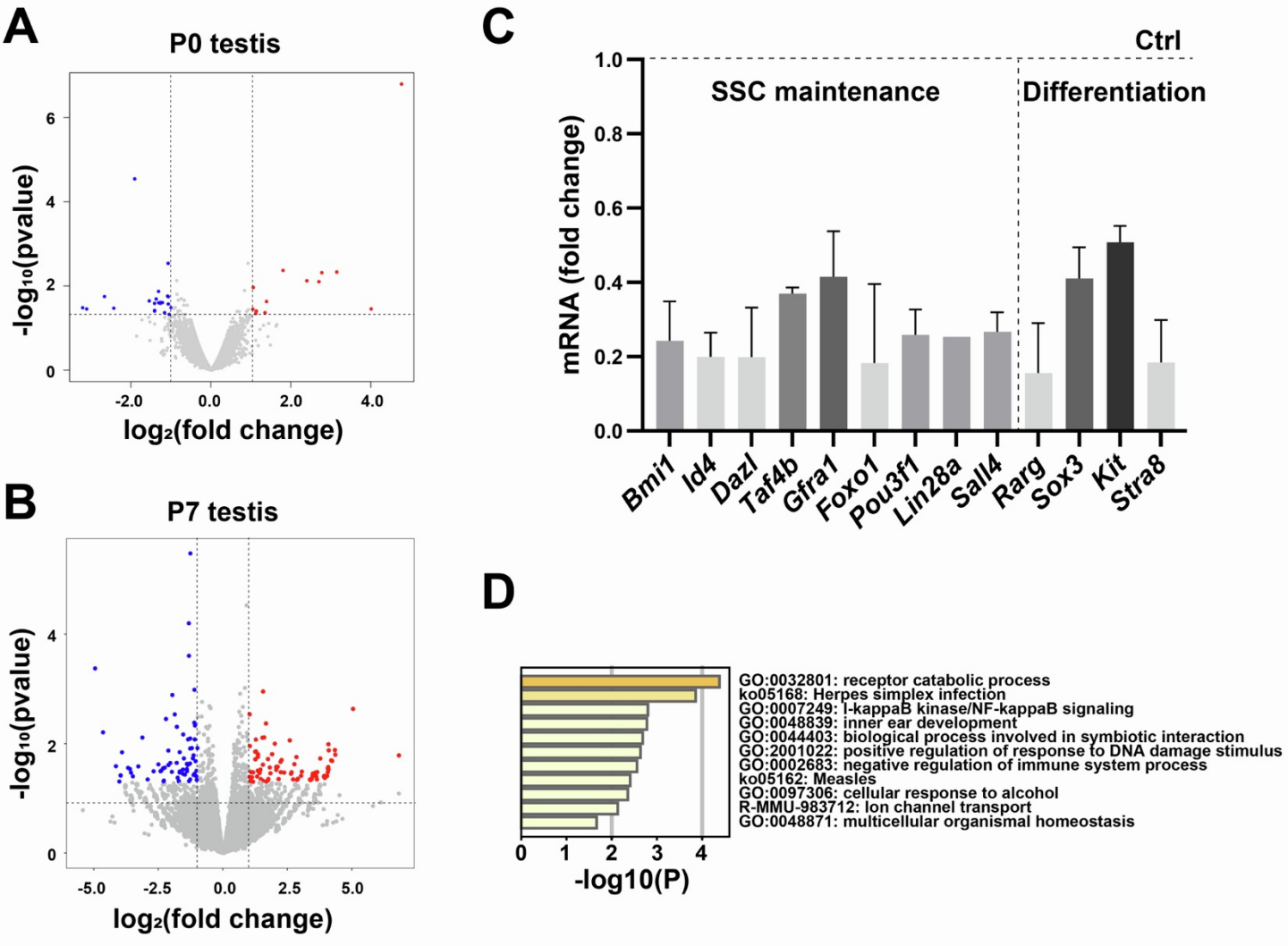

Figure S4. UHRF1 ablation results in the abnormal transcriptome in testes.

(A) Volcano plot showing deregulated genes in *Uhrf1*$^{flox/-}$;*Vasa*-Cre testes at P0. Significantly deregulated genes have a *P*-value of < 0.05 and fold change of > 2. Three biological replicates were indicated.

(B) Volcano plot showing deregulated genes in *Uhrf1*$^{flox/-}$; *Vasa*-Cre testes at P7.

(C) RT-qPCR to verify the downregulated genes associated with SSC homeostasis in *Uhrf1*$^{flox/-}$; *Vasa*-Cre testes at P7.

(D) Gene ontology of upregulated genes in *Uhrf1*$^{flox/-}$; *Vasa*-Cre testes at P7.

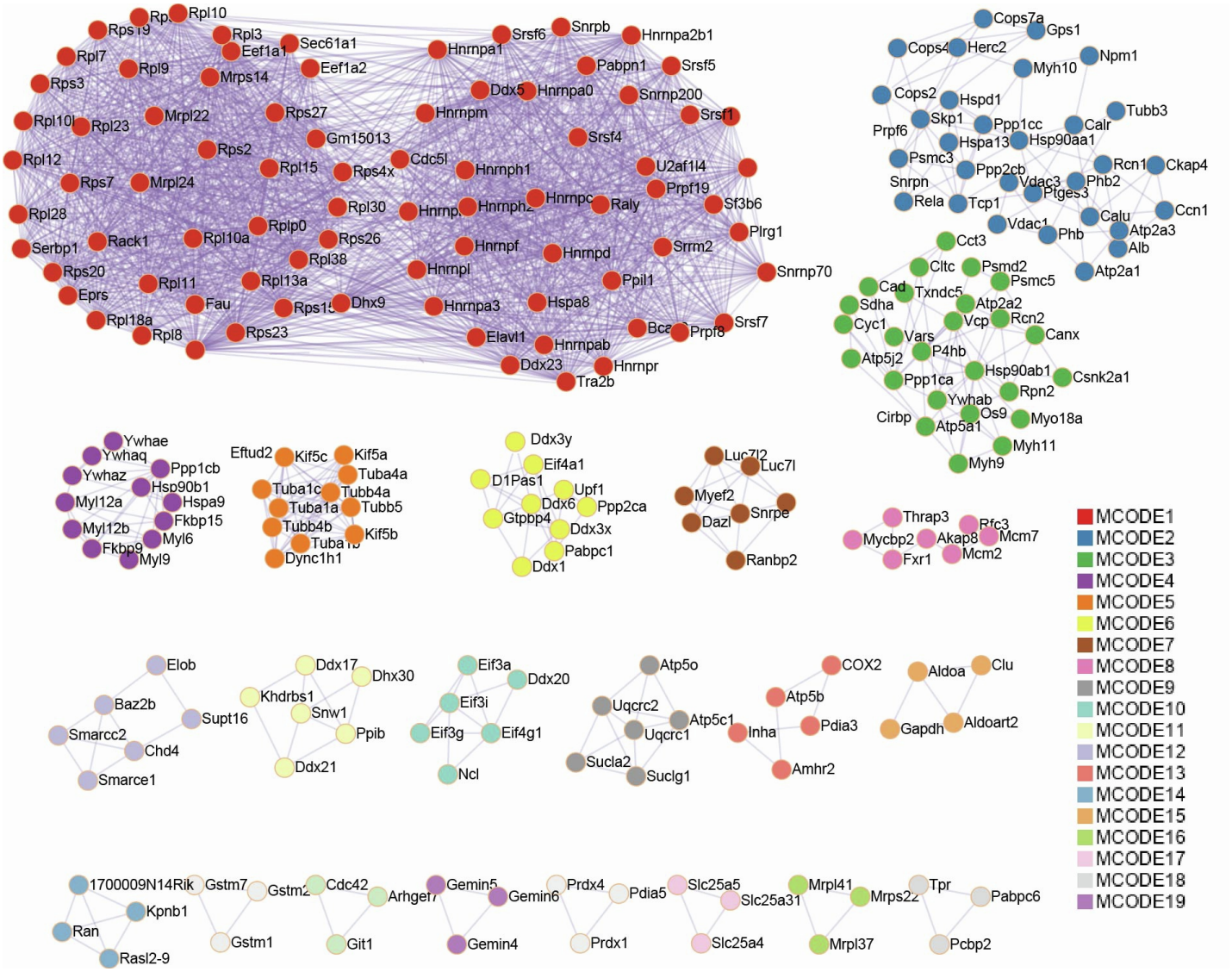

Figure S5. The Protein-Protein Interaction Networks (PPI) analysis of 337 candidate proteins interacted with UHRF1.

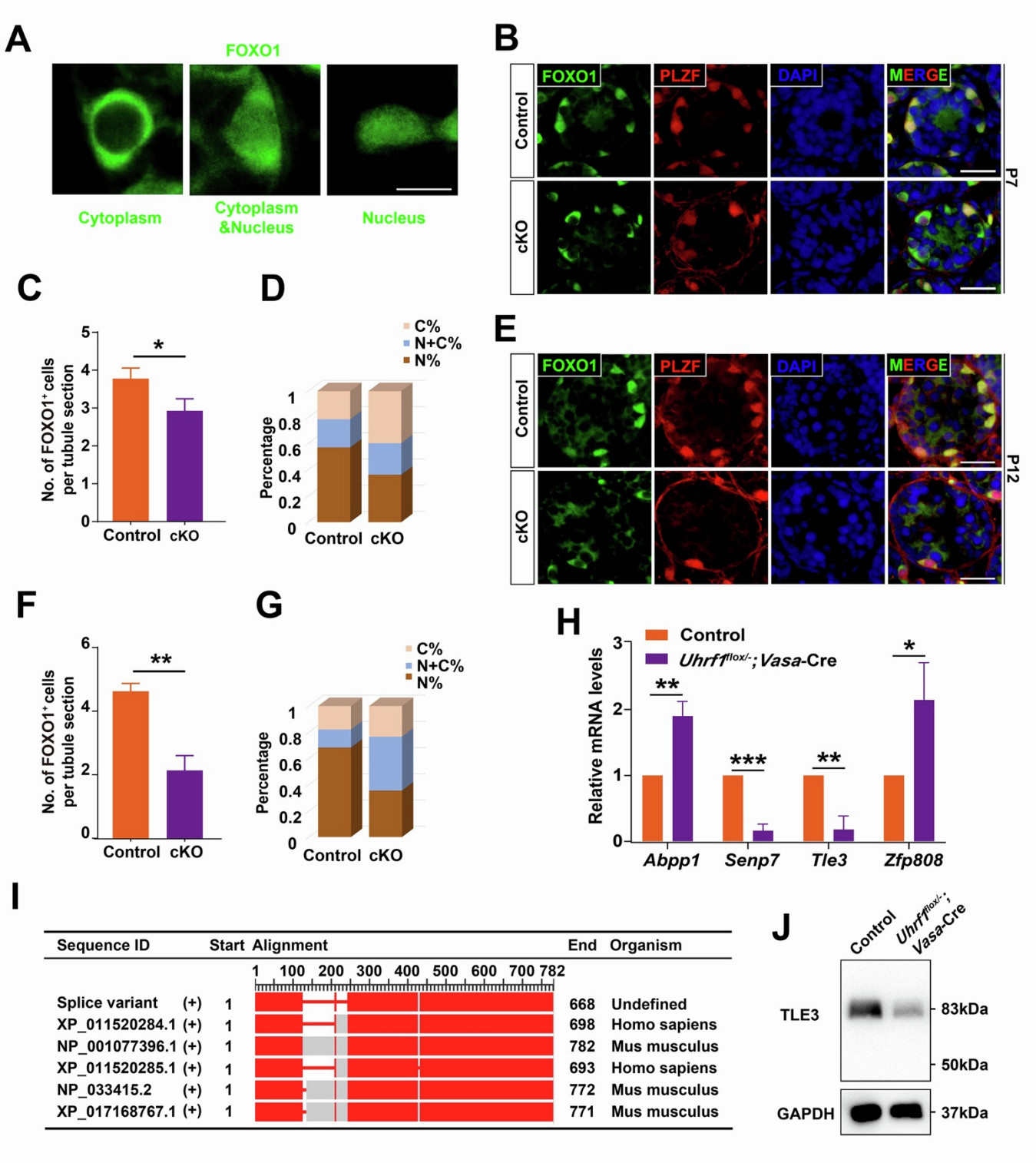

Figure S6. UHRF1 regulates the translocation of FOXO1 expression and alternative splicing in spermatogonia.

(A) Three types of FOXO1 subcellular localization are shown. Scale bars = 50 μm.

(B-G) The co-immunostaining of FOXO1 and PLZF in control and *Uhrf1*$^{flox/-}$; *Vasa*-Cre mouse testes at P7 (B) and P12 (E). Scale bars = 25 μm. The number of FOXO1 positive cells per tubule was significantly decreased in mutant testes (C and F). The subcellular distribution of FOXO1 is disturbed in mutant spermatogonia (D and G).

(H) RT-qPCR analysis of *Apbb1, Senp7, Tle3,* and *Zfp808* expression between control and *Uhrf1*$^{flox/-}$; *Vasa*-Cre testes at P7.

(I) Comparison of predicted ORFs of exon7/8-skipped *Tle3* isoforms with sequence databases.

(J) Western blot of *Tle3* protein in P7 control and *Uhrf1*$^{flox/-}$; *Vasa*-Cre testes using GAPDH as load control.

Supplemental Tables

Table S1. The differential expressed genes identified from P0 testes in *Uhrf1* cKO mice were determined by RNA-Seq, related to Figure 4 and Figure S4.

See supplemental Excel file.

Table S2. The differential expressed genes identified from P7 testes in *Uhrf1* cKO mice were determined by RNA-Seq, related to Figure 4 and Figure S4.

See supplemental Excel file.

Table S3. A total of 337 UHRF1 interacting proteins were identified by IP/MS, related to Figure 5 and Figure S5.

See supplemental Excel file.

Table S4. The GO term identified from UHRF1-interacting proteins, related to Figure 5 and Figure S5.

See supplemental Excel file.

Table S5. Alternative splicing events identified from *Uhrf1* cKO and control testes at P7 were determined by RNA-seq, related to Figure 6.

See supplemental Excel file.

Table S6. The primer sequences and antibodies used in this study, related to Experimental Procedures.

See supplemental Excel file.